CHAPTER 6:
STUDY ON MECHANICAL STRENGTH OF CONCRETE

6.1 GENERAL

It is vital that every rigid pavement should keep on performing its designed functions i.e. to disperse the vehicular load stresses over a wide area with small depth. Performance of concrete is dictated by its durability properties as well as mechanical properties. Both mechanical properties and durability properties of concrete play an equally important role in providing resistance to the processes of deterioration over the expected service life.

The physical properties that concrete displays upon the application of forces are known as mechanical properties. The mechanical strength of concrete signifies the maximum amount of stresses it can withstand. The concrete having high strength can be associated with good quality. Pavement Quality Concrete (PQC) is a concrete having sufficient quality such that it can be used as the surfacing on rigid pavements. In the present study, PQC was designed for grade of M40. The compressive, flexural and split tensile strength of the M40 grade concrete admixed with RSA and MS were found out and various equations between these parameters were established. Also, the mineralogical characteristics of concrete were studied by XRD analysis while microstructural characteristics of concrete were observed by SEM as well as petrography analysis.

6.2 MIX PROPORTIONS FOR TESTING ON CEMENT CONCRETE

In the previous chapter, it was concluded that the compressive strength of mortar admixed with RSA rises up to 5% replacement of OPC (R5) and then decreases on further replacement. The compressive strength at 10% replacement was lower than

the strength at 5% replacement but was higher than the control mix R0 (100% OPC). Mortar of mix R5 (5% RSA) was already showing improved strength properties while properties of mortar of mix R10 were at the borderline. Therefore only mix R10 (10% RSA) was selected for further testing based on the hypothesis that concrete of mix R5 would have shown improved mechanical and durability properties while there was uncertainty about the properties of concrete of mix R10.

To study the effect of admixing MS on mechanical and durability properties of concrete, 4 mixes were selected: M2.5 (2.5% MS), M5 (5% MS), M7.5 (7.5% MS) and M10 (10% MS). Similarly, to study the effect of admixing composite of RSA and MS, 4 mixes were selected: R5M5 (5% RSA, 5% MS), R5M7.5 (5% RSA, 7.5% MS), R10M5 (10% RSA, 5% MS) and R10M7.5 (10% RSA, 7.5% MS).

6.3 MIX DESIGN OF M40 GRADE PQC

The w/b ratio was kept fixed at 0.39. The mix design of concrete having characteristic cube compressive strength of 40 MPa at 28 days are given in Table 6.1. The ratio between amount of coarse aggregates and fine aggregates was finalized at 0.65 and 0.35, respectively. The ratio between amount of 20 mm and 10 mm maximum nominal size coarse aggregates was maintained at 0.6 and 0.4 respectively. Based on these ratios, the overall combined gradation of aggregates was verified with the limits specified in IRC 44 [226]. The combined gradation of aggregates is shown in Table 6.2. The reduction in workability was compensated by using superplasticizer. The dosage of HRWR for each mix (Table 6.1) was decided by slump test, keeping the slump at 50 ± 10 mm.

Table 6.1 Quantity of materials (kg) per m^3 of concrete

Mix	Binder			Aggregate	Water	HRWR
	OPC	RSA	MS			
R0	406	-	-	1913	158	1.624
R10	365.4	40.6	-	1913	158	6.09
M2.5	395.85	-	10.15	1913	158	3.654
M5	385.7	-	20.3	1913	158	4.263
M7.5	375.55	-	30.45	1913	158	4.872
M10	365.4	-	40.6	1913	158	5.278
R5M5	365.4	20.3	20.3	1913	158	6.902
R5M7.5	355.25	20.3	30.45	1913	158	8.12
R10M5	345.1	40.6	20.3	1913	158	9.744
R10M7.5	334.95	40.6	30.45	1913	158	10.15

Table 6.2 Percentage passing of coarse and fine aggregates for PQC

Sieve Size (mm)	Percentage Passing		
	Min.	Max.	Obtained
20	90	100	98.77
10	48	78	63.67
4.75	30	58	34.69
0.6	8	35	19.11
0.15	0	12	2.45
0.075	0	5	0.77

6.4 COMPRESSIVE STRENGTH

Most of the times, the results of compressive strength test of concrete are used for determining whether the mixture of concrete meets the stipulations mentioned in the standard specifications. Compressive strength is one of the fundamental mechanical properties of concrete. The evolution of concrete strength helps in deciding the steps involved in the construction of a rigid pavement and also helps in estimating the time needed for its construction [285]. The effects of replacement of OPC by MS and RSA on the compressive strength of the M40 grade pavement quality concrete can be observed in Table 6.3 and Figure 6.1. The relative percentage change in compressive strength of concrete (admixed with different proportions of RSA and MS) as compared to control concrete (R0) at various ages of curing is given in Table 6.4 and shown in Figure 6.2.

Table 6.3 Compressive strength of concrete

Mix	Compressive Strength (MPa)					
	3 days	7 days	28 days	60 days	90 days	365 days
R0	27.55	37.00	48.77	52.00	52.93	53.04
R10	27.59	37.20	48.88	52.52	53.04	53.56
M2.5	28.09	38.00	53.02	55.01	55.70	56.16
M5	28.80	38.80	54.08	55.93	56.50	57.20
M7.5	29.15	39.20	55.01	56.62	57.31	57.66
M10	26.31	32.80	51.07	54.08	55.12	55.93
R5M5	27.91	37.80	50.96	53.38	54.08	55.23
R5M7.5	28.54	38.70	53.61	55.46	56.16	56.62
R10M5	27.64	37.70	48.99	53.04	53.97	54.08
R10M7.5	27.74	37.74	49.22	53.21	54.03	54.60

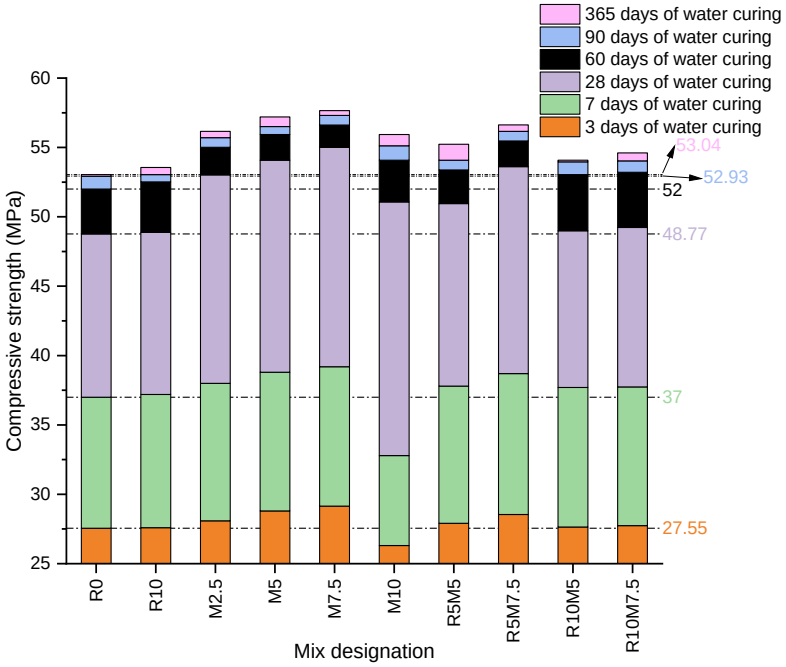

Figure 6.1 Graphical comparison of compressive strength of concrete at various ages of water curing

Table 6.4 Percentage change in compressive strength of admixed concrete w.r.t. control concrete (R0)

Mix	Change in Compressive Strength (%)					
	3 days	7 days	28 days	60 days	90 days	365 days
R10	+0.15	+0.53	+0.23	+1.00	+0.21	+0.98
M2.5	+1.95	+2.70	+8.71	+5.78	+5.24	+5.88
M5	+4.54	+4.86	+10.89	+7.56	+6.75	+7.84
M7.5	+5.81	+5.93	+12.79	+8.88	+8.28	+8.71
M10	-4.49	-11.4	+4.73	+4.00	+4.14	+5.45
R5M5	+1.31	+2.16	+4.49	+2.66	+2.17	+4.14
R5M7.5	+3.58	+4.59	+9.93	+6.66	+6.10	+6.75
R10M5	+0.33	+1.89	+0.46	+2.00	+1.96	+1.96
R10M7.5	+0.68	+1.99	+0.93	+2.32	+2.07	+2.94

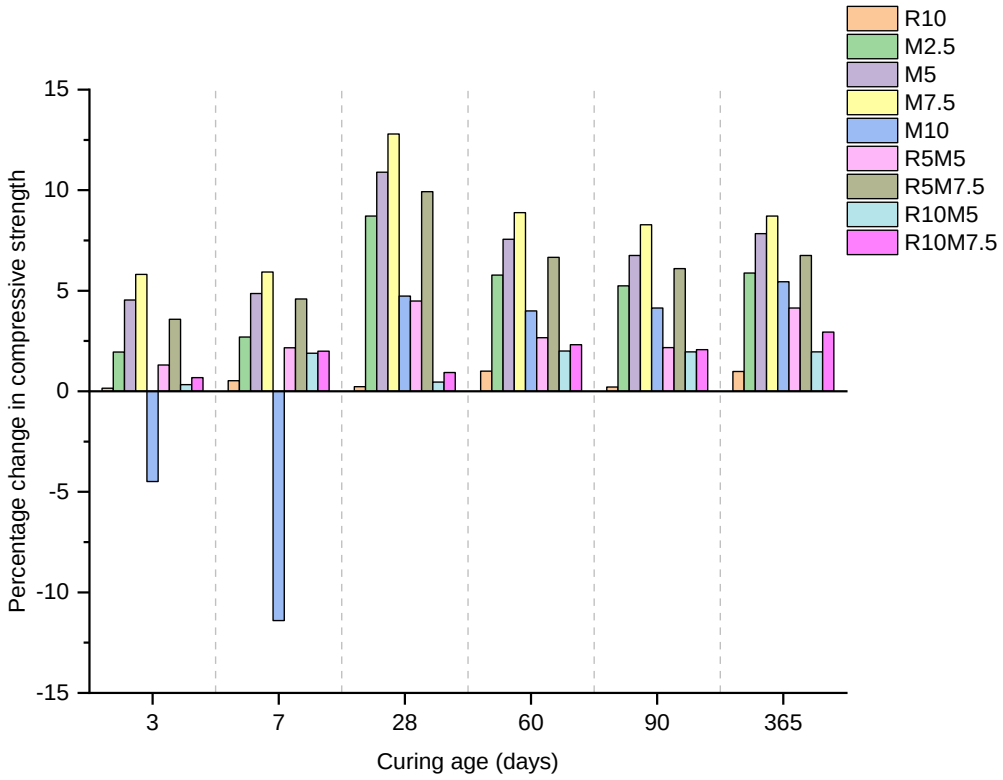

Figure 6.2 Relative percentage change in compressive strength of admixed concrete w.r.t. control concrete (R0)

The replacement of OPC by microsilica increased the strength of the M40 grade pavement quality concrete to a great extent as can be observed in Table 6.3 and Figure 6.1. The substantial increase in surface area, because of the addition of microsilica in the concrete, causes a corresponding rise in internal surface forces, which indirectly increases the cohesiveness of the concrete [23]. Therefore, the mixtures containing microsilica had higher compressive strength because as a result of cohesiveness, no. of voids decreases. Mix M10 at 3 and 7 days of curing in water had less compressive strength than the control mix R0. It was the only mixture which had lower strength (at early days of curing) than the control mix as the % change in compressive strength w.r.t. to the control mix was negative (Table 6.4 and Figure 6.2). It was because as percentage of microsilica in the mix increases, the amount of SO_3 also increases subsequently decreasing the amount of alite and aluminate content and increasing the

belite content [286]. Therefore compressive strength reduces at early stages of curing due to the reduction in the amount of alite and increases at later stages of curing due to the increase in the amount of belite. M7.5 (7.5% microsilica) had the highest compressive strength amongst all the mix. Mix R10 did show an increase in the strength, but the percentage increase w.r.t the control mix was less than 1% (Table 6.4). Maximum strength gain in R10 over R0 was at 60 days of curing in water.

Amongst the mixes containing a composite of microsilica and rice straw ash, R5M7.5 shows the maximum strength. In Table 6.3 & 6.4 and Figure 6.1 & 6.2, it can be seen that addition of microsilica increases the compressive strength, but the addition of rice straw ash decreases the compressive strength though it remains more than the compressive strength of R0. For instance, the compressive strength of R5M5 at 3 days of curing in water was 27.91 MPa while the compressive strength of R10 was 27.59 MPa. It was observed that if 5% microsilica of mix R5M5 (5% rice straw ash, 5% microsilica) was replaced by 5% rice straw ash, there was a decrease in the compressive strength of the resulting mix R10 (10% rice straw ash) w.r.t mix R5M5 but remained higher than the control mix R0. Similar trends were also observed at 7, 28, 60, 90 and 365 days of curing. The relative percentage increase in the compressive strength of the mix R5M5 and mix R10 w.r.t. control mix R0 decreases from 1.31 to 0.15%, 2.16 to 0.53%, 4.49 to 0.23%, 2.66 to 1%, 2.17 to 0.21% and 4.14 to 0.98% at 3, 7, 28, 60, 90 and 365 days of curing respectively.

With the increase in the ratio of RSA in the mix, the amount of the unburned carbon in the concrete mix also increases thus leading to increased water affinity of the concrete. It was one of the factors for reduction in the strength of concrete admixed with MS when the amount of RSA was increased. The physical and chemical

properties of concrete are affected by Magnesium Oxide (MgO) content in cement or supplementary cementitious material like RSA and MS. According to Mazurok et al. (2017) [287], the strength of concrete decreases with increase in the MgO content of OPC because the hydration of cement in the presence of MgO leads to the formation of Magnesium Hydroxide ($Mg(OH)_2$) which does not have adequate strength. According to Borhan and Al-Rawi (2016) [141], the formation of $Mg(OH)_2$ causes internal stresses in the concrete, thus decreasing its strength. They concluded that the stresses were caused because of delayed expansion in concrete due to the formation of $Mg(OH)_2$. Also, the optimum gypsum content of cement reduces with an increase in the amount of MgO content [141]. The amount of MgO in MS was less than RSA (Table 4.4), and thus MS admixed concrete gave higher compressive strength as compared to the RSA admixed concrete. The most suitable amount of MgO in the cement was found to be in the range of 2-3%. It was mainly due to the better fluidity effect of the MgO at this range [288].

6.5 FLEXURAL STRENGTH

Reinforced concrete is by a long shot, much superior to either steel or concrete independently and is stronger in both compression as well as tension. Plain concrete is weak in tension due to its brittle nature and approximately ten times stronger in compression [289]. Therefore, the tensile strength is preferred over compressive strength for the mix design of concrete for rigid pavements (reinforcements are only occasionally used in rigid pavements) however it is not mandatory. The effects of RSA, MS and their composite on flexural strength of the admixed concrete are given in Table 6.5 and shown in Figure 6.3. The relative percentage changes in flexural strength of

admixed concrete as compared to control concrete (R0) at various days of curing are given in Table 6.6 and shown in Figure 6.4.

Table 6.5 Flexural strength of concrete

Mix	Flexural Strength (MPa)					
	3 days	7 days	28 days	60 days	90 days	365 days
R0	4	4.8	5.62	6.3	6.4	6.45
R10	4.02	4.9	5.65	6.35	6.45	6.5
M2.5	4.4	5.2	5.9	6.65	6.7	6.8
M5	5	5.8	6.24	6.7	6.8	6.85
M7.5	5.1	6	6.5	6.8	6.9	6.95
M10	3.86	4.6	5.8	6.6	6.65	6.75
R5M5	4.3	5.1	5.75	6.55	6.6	6.7
R5M7.5	4.8	5.7	6.07	6.67	6.73	6.81
R10M5	4.1	4.95	5.67	6.45	6.5	6.6
R10M7.5	4.25	5	5.7	6.5	6.55	6.65

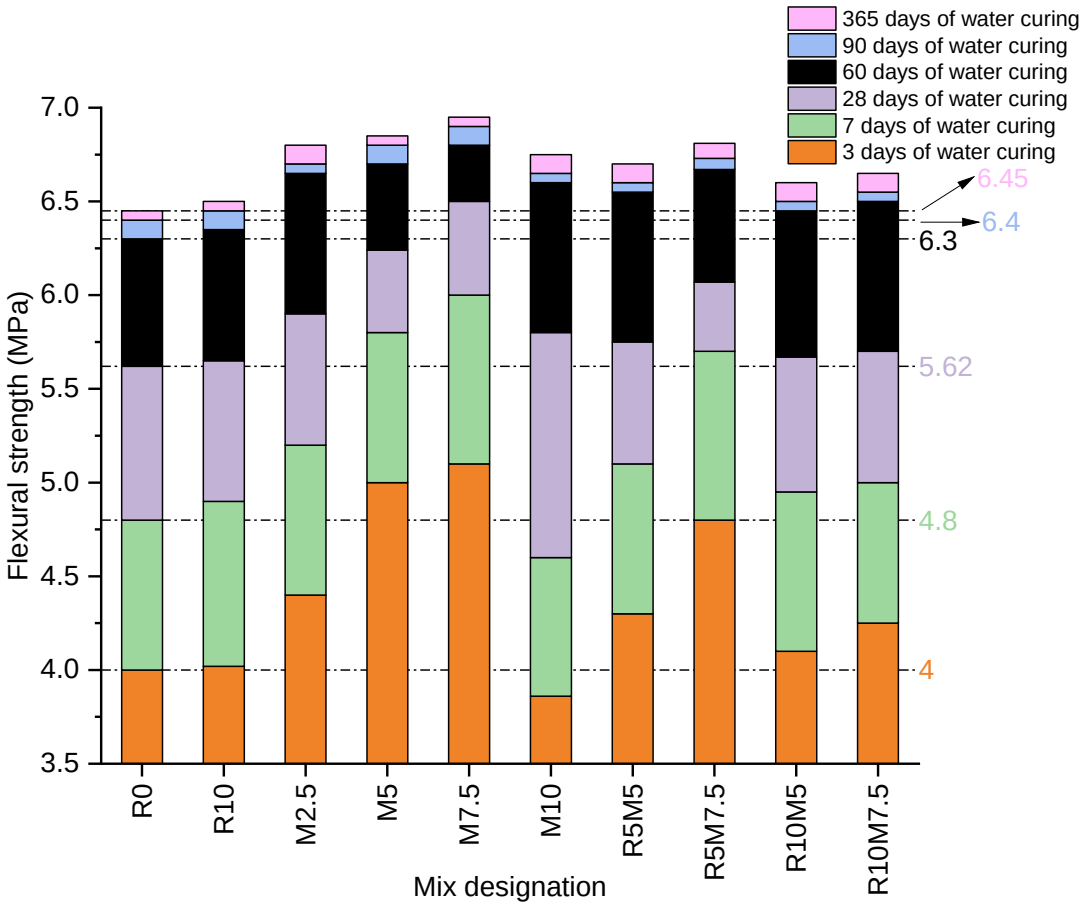

Figure 6.3 Graphical comparison of flexural strength of concrete at various ages of water curing

Table 6.6 Percentage change in flexural strength of admixed concrete w.r.t. control concrete (R0)

Mix	Change in Flexural Strength (%)					
	3 days	7 days	28 days	60 days	90 days	365 days
R10	+0.5	+2.08	+0.53	+0.79	+0.78	+0.78
M2.5	+10	+8.33	+4.98	+5.56	+4.69	+5.43
M5	+25	+20.83	+11.03	+6.35	+6.25	+6.20
M7.5	+27.5	+25.00	+15.66	+7.94	+7.81	+7.75
M10	-3.5	-4.17	+3.20	+4.76	+3.91	+4.65
R5M5	+7.5	+6.25	+2.31	+3.97	+3.12	+3.88
R5M7.5	+20	+18.75	+8.01	+5.87	+5.16	+5.58
R10M5	+2.5	+3.13	+0.89	+2.38	+1.56	+2.33
R10M7.5	+6.25	+4.17	+1.42	+3.17	+2.34	+3.10

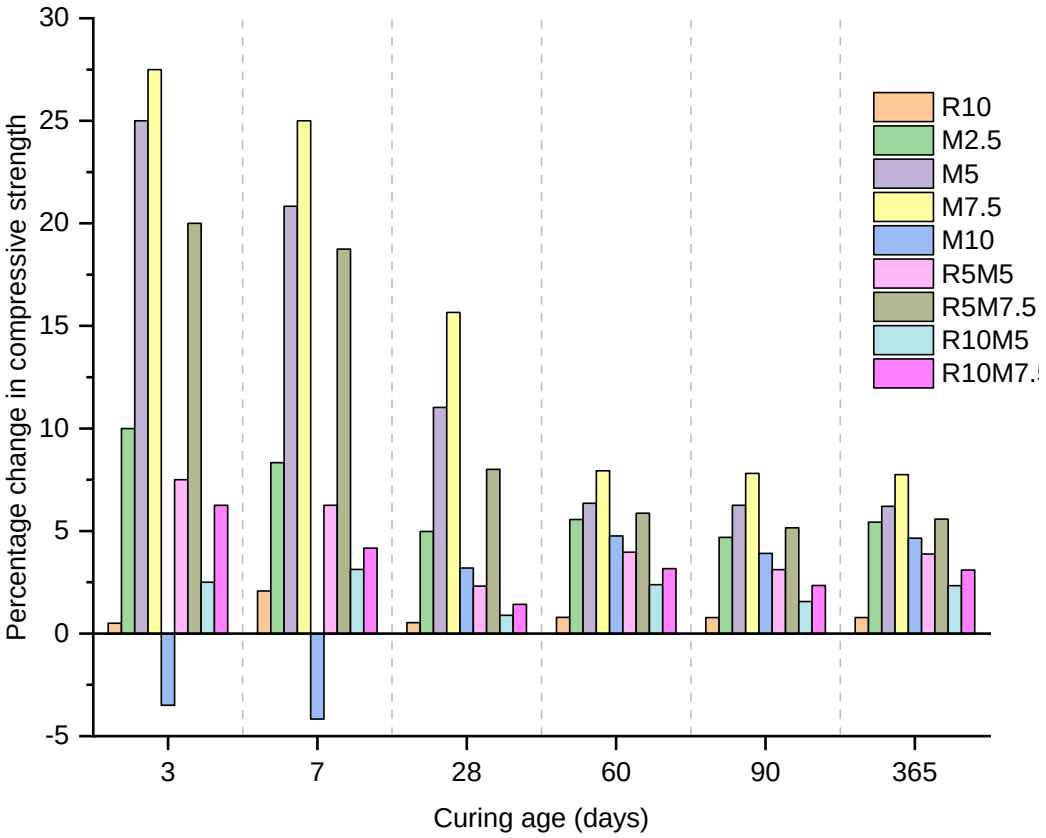

Figure 6.4 Relative percentage change in flexural strength of admixed concrete w.r.t. control concrete (R0)

Similar to compressive strength, flexural strength also increases with an increase in the percentage of microsilica in the concrete. The flexural strength of the mix M10 (at 3 and 7 days of curing in water) was also less than that of the control mix R0. But at 28, 60, 90 and 365 days of curing, the flexural strength of M10 was more than that of

the R0 similar to the results of compressive strength test. It was because of the absence of alite, which is responsible for strength at the early days of curing and also because of the presence of belite, which is responsible for strength at later stages. Amongst the concrete mixes containing a composite of mineral admixtures, flexural strength of R5M7.5 was highest while amongst all the concrete mixes tested in this study, flexural strength of M7.5 was highest at each day of curing in water.

The effect of RSA and MS was more profound on the flexural strength of concrete at 3 and 7 days of curing as compared to other days of curing while they affected compressive strength mostly at 28, 60, 90 and 365 days of curing (Figure 6.2 and 6.4). For example, the percentage increase in the compressive strength of concrete mix M2.5 w.r.t control concrete R0 was 1.95% and 2.70% at 3 and 7 days of curing respectively while the percentage increase in flexural strength for the same was 10% and 8.33% respectively . The percentage increase in compressive strength for the same at 28, 60, 90 and 365 days of curing was 8.71%, 5.78%, 5.24%, and 5.88% respectively whereas the percentage increase in flexural strength for the same was 4.98%, 5.56%, 4.69%, and 5.43% respectively. Therefore it can be said that the RSA and MS affect mostly flexural strength at early days of curing and compressive strength at later days of curing.

6.6 SPLIT TENSILE STRENGTH

In general, there are two types of tensile strength: flexural strength and split tensile strength. In the previous section, the effects of RSA, MS and their composite on flexural strength of concrete was discussed. The effects of admixing RSA and MS on split tensile strength of the concrete are given in Table 6.7 and shown in Figure 6.5. The relative percentage changes in split tensile strength of admixed concrete as compared to

control concrete (R0) at various ages of curing are given in Table 6.8 and shown in Figure 6.6.

Table 6.7 Split tensile strength of concrete

Mix	Split Tensile Strength (MPa)					
	3 days	7 days	28 days	60 days	90 days	365 days
R0	2.26	2.97	3.89	4.12	4.2	4.25
R10	2.3	2.99	3.95	4.19	4.25	4.27
M2.5	2.55	3.18	4.17	4.42	4.5	4.52
M5	2.9	3.46	4.53	4.81	4.9	4.93
M7.5	3.2	3.68	4.81	5.09	5.16	5.2
M10	2.47	3.11	4.39	4.65	4.75	4.8
R5M5	2.4	3.11	4.03	4.27	4.35	4.4
R5M7.5	2.87	3.44	4.23	4.75	4.85	4.9
R10M5	2.33	3.01	3.99	4.23	4.3	4.32
R10M7.5	2.37	3.04	4	4.24	4.32	4.35

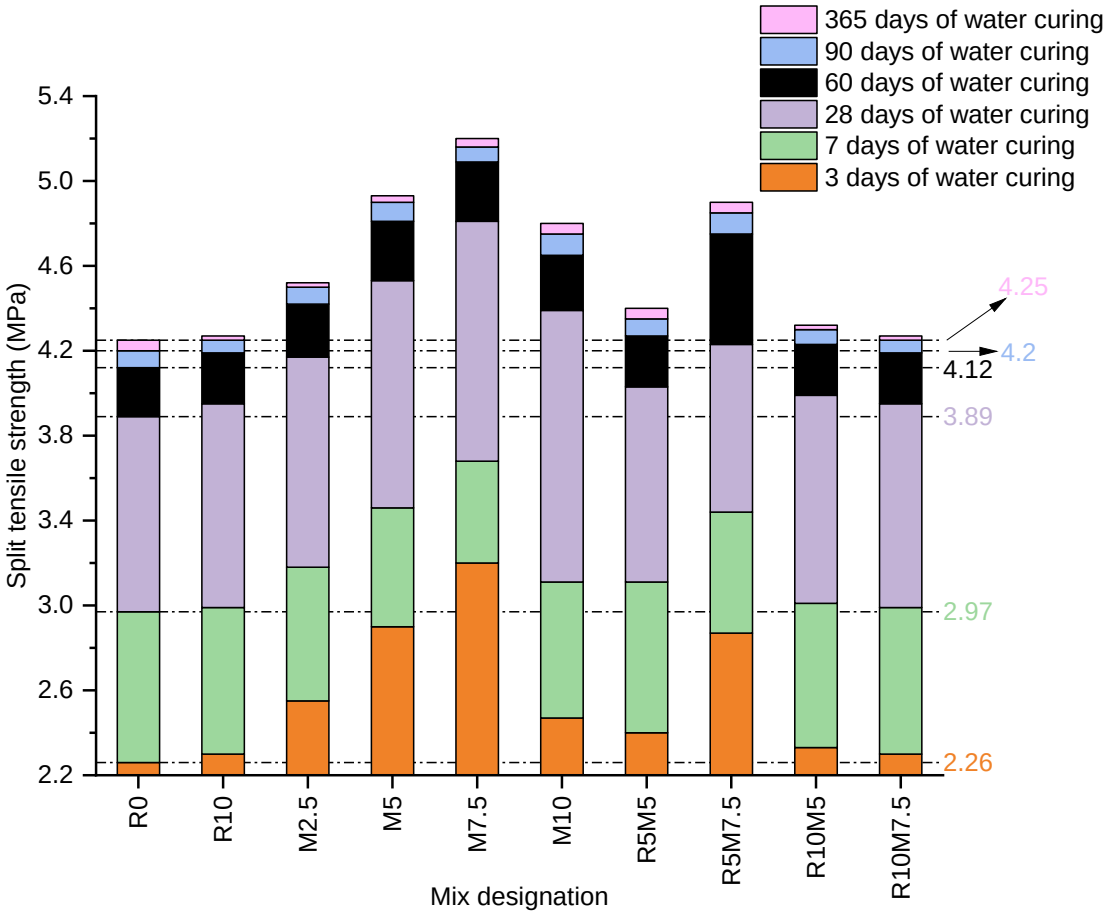

Figure 6.5 Graphical comparison of split tensile strength of concrete at various ages of water curing

Table 6.8 Percentage change in split tensile strength of admixed concrete w.r.t. control concrete (R0)

Mix	Change in Split Tensile Strength (%)					
	3 days	7 days	28 days	60 days	90 days	365 days
R10	1.77	0.67	1.54	1.70	1.19	0.47
M2.5	12.83	7.07	7.20	7.28	7.14	6.35
M5	28.32	16.50	16.45	16.75	16.67	16.00
M7.5	41.59	23.91	23.65	23.54	22.86	22.35
M10	9.29	4.71	12.85	12.86	13.10	12.94
R5M5	6.19	4.71	3.60	3.64	3.57	3.53
R5M7.5	26.99	15.82	8.74	15.29	15.48	15.29
R10M5	3.10	1.35	2.57	2.67	2.38	1.65
R10M7.5	4.87	2.36	2.83	2.91	2.86	2.35

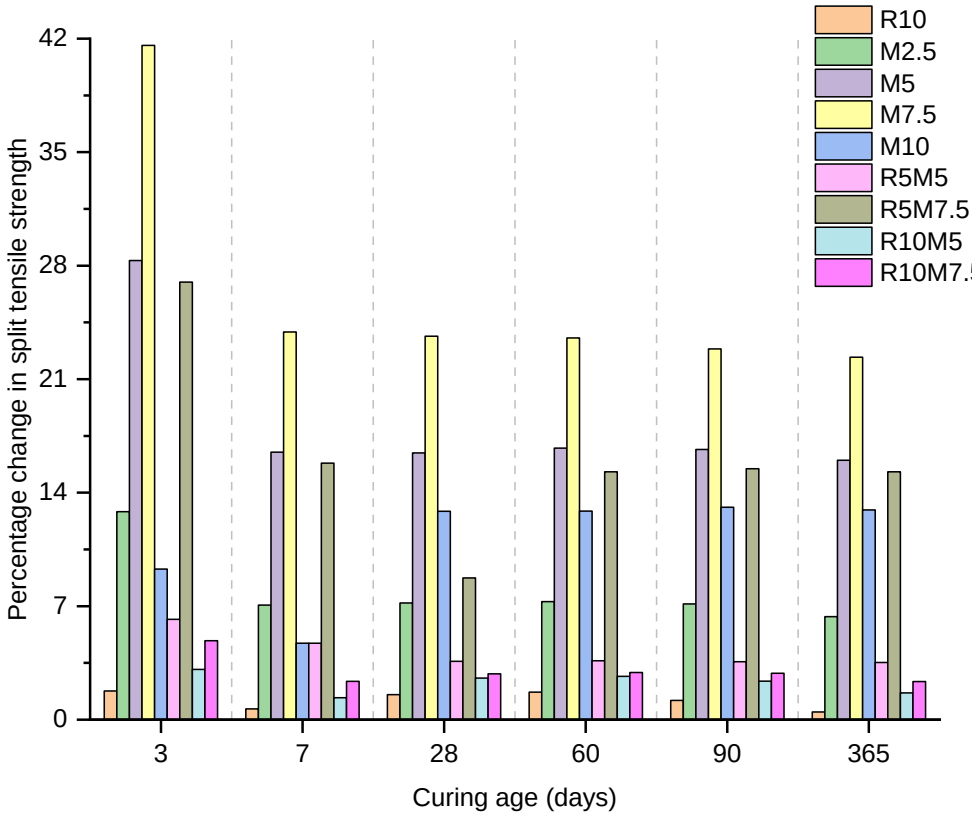

Figure 6.6 Relative percentage change in split tensile strength of admixed concrete w.r.t. control concrete (R0)

Similar to compressive and flexural strength, split tensile strength also increases with an increase in the percentage of microsilica in the mixture. Unlike the results of compressive and flexural strength test, the split tensile strength of M10 was higher than that of the control mix R0 at 3 and 7 days of curing in water. Thus it can be said that amount of SO_3 in microsilica did not affect the split tensile strength of M10. The split

tensile strength of R5M7.5 was highest amongst the concrete mixes containing a composite of RSA and MS while split tensile strength of M7.5 was highest amongst all the concrete mixes tested in this study at each day of curing in water.

The results found in compressive strength test, flexural strength test and split tensile strength test of each concrete specimen followed a similar pattern. It can be seen in Table 6.4, 6.6 and 6.8 that RSA and MS mostly affected split tensile strength at all ages of curing in water (except 7 days curing) while at 7 days of curing, mostly flexural strength was affected due to admixing of RSA and MS. Due to admixing of RSA or MS, the percentage changes in flexural and split tensile strength were highest at 7 and other days of curing respectively. For instance, the percentage increase in the flexural and split tensile strength of concrete mix M5 was 25% and 28.32% respectively at 3 days of curing, 20.83% and 16.5% respectively at 7 days of curing, 11.03% and 16.45% respectively at 28 days of curing.

6.7 MINERALOGICAL ANALYSIS OF CONCRETE

The mineralogical analysis of hardened concrete, in powdered form by a rapid analytical technique known as X-ray Diffraction (XRD), was done to study the crystalline structure of the components of the concrete and to determine the reasons behind the development of strength in the concrete due to admixing of RSA and MS. For mineralogical analysis, only six mixes (R0, R10, R5M5, R5M7.5, R10M5 and R10M7.5) at 28 days of curing were chosen. XRD diffractograms of concrete of various mixes is shown in Figure 6.7.

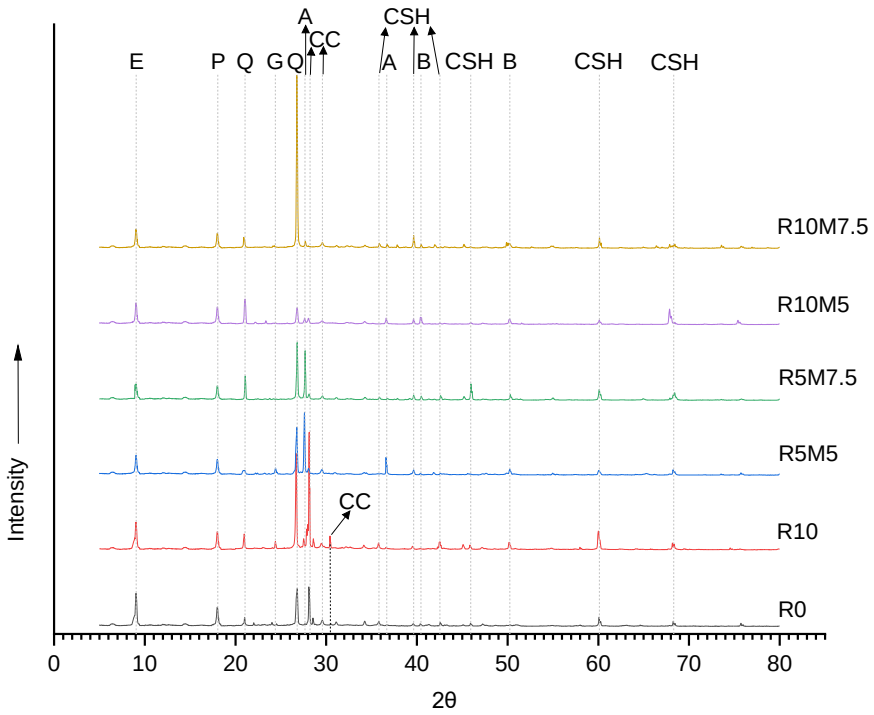

Figure 6.7 XRD diffractograms of control concrete (R0) and concrete of mix R10, R5M5, R5M7.5, R10M5 and R10M7.5

(E - Etrringite; P – Portlandite; Q – Quartz; G – Gypsum; A – Alite; CC – Calcite; CSH – Calcium Silicate Hydrate; B – Belite;)

The formation of hydrated compounds like calcite, portlandite, and calcium silicate hydrate is clearly visible is XRD analysis of all the concrete mixes (Figure 6.7). The peaks of C-S-H were most prominent in the mix R5M7.5 when compared with other mixes justifying the maximum strength of R5M7.5 among the six mixes which were analysed by XRD technique. The increase in the amount of C-S-H gel in all the mixes as compared to R0 was due to consumption of portlandite by the pozzolanic action of RSA and MS. It can also be justified by reduction in the intensity of peaks of portlandite. It was the main reason behind increase in the strength of all the mixes of admixed concrete as compared to the control concrete. The peaks of calcite were limited to control mix (R0) as well as concrete mix containing only RSA (R10) however these peaks were diminished when MS was also added to the concrete admixed with RSA. It was because admixing of MS reduces the rate of carbonation of

portlandite due to its higher pozzolanicity as compared to RSA (an ability which can be associated with rapid consumption of portlandite). This result was at par with the XRD analysis of cement paste admixed with RSA (Figure 5.7) in which it was concluded that RSA increases the rate of carbonation. The identification of amorphous C-S-H by XRD analysis is difficult due to the presence of calcite in the hydrated samples because the XRD peaks corresponding to calcite overlap those corresponding to amorphous C-S-H. But, in this investigation, few sharp peaks of C-S-H found were the characteristic peaks of tobermorite (C-S-H in crystalline form). The positive effect of tobermorite on the cementitious systems has been well-documented in the past by many authors. Also, being crystalline, it can be easily detected in the XRD analysis. The peaks of gypsum were also found in R0 however with low intensity due to their transformation to ettringite. This intensity reduced further with the admixing of MS and RS. Few peaks of quartz (SiO_2) were also observed however they were not part of the hydration products. Their presence could be attributed to the presence of siliceous sand, RSA and MS. Absence of peaks of unhydrated compounds like alite and belite in XRD diffractogram of control concrete (R0) implies that control concrete attains most of its strength at 28 days of curing. However, these peaks were prolonged in admixed concrete especially in mix R5M5 and R5M7.5 which signifies that the strength of concrete admixed with RSA and MS will continue to grow even at later days of curing.

6.8 MICROSTRUCTURAL ANALYSIS OF CONCRETE

6.8.1 SEM Analysis

A Scanning Electron Microscope (SEM) produces images of the microstructure of concrete by scanning its surface by the focused beams of electrons [290]. The images produced by SEM helps in studying the topography of concrete surface and also, the

products formed due to hydration reaction. The SEM images also help in analysing the effect of admixing mineral admixtures on the hardened cement paste. Similar to the samples studied by XRD analysis, only six mixes (R0, R10, R5M5, R5M7.5, R10M5 and R10M7.5) at 7, 28 and 90 days of curing were chosen for their microstructural analysis by SEM. Various phases in SEM micrographs of concrete microstructure were identified based on the findings of extensive past studies.

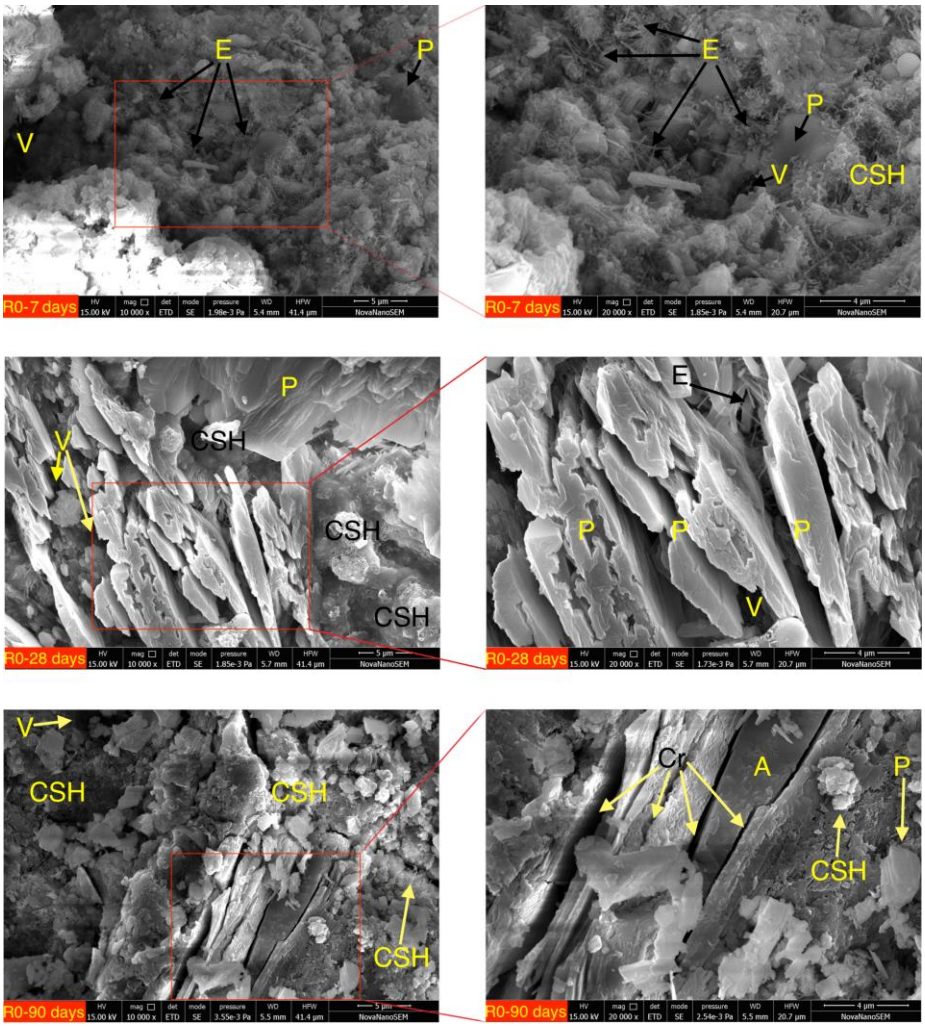

Figure 6.8 SEM micrograph of control concrete (R0) at 7, 28 and 90 days of curing at 10,000 (left) and 20,000 (right) times magnification levels

(V – Void; E – Ettringite; P – Portlandite; CSH – Calcium Silicate Hydrate; A – Aggregate, Cr – Cracks in the aggregate)

Figure 6.8 shows the SEM micrograph of the control concrete (R0) at 10,000 and 20,000 times magnification level. Abundant amount of voids (V) were observed in

R0 at 3 days of curing and were reduced when curing age was increased up to 90 days due to formation of hydration products like C-S-H gel and portlandite. The C-S-H gel was characterized by equant grains, forming a foil-like sheet while $Ca(OH)_2$ was identified by their blocky crystals in the present work. The presence of voids reduces the strength of the concrete [160]. The C-S-H gel fills the void and increases the compactness and strength of the concrete matrix [291] and portlandite affects the strength of concrete by reducing the volume of the pores. This change in volume of pores is basically because portlandite converts a portion of water present in pores to solid form [292]. However, the increase in strength due to portlandite formation as compared to C-S-H gel formation is less significant. Also, due to high solubility of portlandite, its presence increases the chances of leaching attack on concrete [293]. The increase in the amount of C-S-H gel and portlandite ($Ca(OH)_2$) can be confirmed from SEM micrograph of R0 (Figure 6.8) and can be easily correlated with increase in strength of R0 with curing age. In the SEM micrograph of R0 at 90 days of curing, large cracks (Cr) in the aggregates (A) were observed. These cracks could have occurred during the process of compaction and filling of fresh concrete into the mould. Large amount of needle like crystals of Ettringite (E) can be observed in SEM micrograph of R0 at 3 days of curing. The ettringite formed during first few hours of cement hydration is generally known as 'primary ettringite' (AFt phase, $C_3A.3CaSO_4.32H_2O$). It is formed due to reaction of gypsum and other sulphate compounds (such as sulphates of sodium, potassium and calcium) with C_3A (Calcium Aluminate) in the presence of water. The formation of 'primary ettringite' is responsible for the stiffening of the fresh cement paste [294]. With the increase in curing age of concrete, primary ettringite disperses into calcium aluminate monosulphate (AFm phase, $C_3A.CaSO_4.12H_2O$) in the presence of moisture [295]. This

is because during the initial stages of hydration (few hours), the ratio between alumina (from C_3A) and sulphate (from $CaSO_4$) is low, as sulphate (SO_4^{2-}) is easily available to dissolve while most of the alumina is contained within the cement particles and does not take part in the hydration reaction in the absence of water (process leading to formation of ettringite). With increase in the duration of hydration of cement, more and more alumina is released into the mix thereby increasing the ratio between alumina and sulphate and converting ettringite into calcium aluminate monosulphate. It was the main reason behind very little presence of ettringite in mix R0 at late days of curing (28 and 90 days).

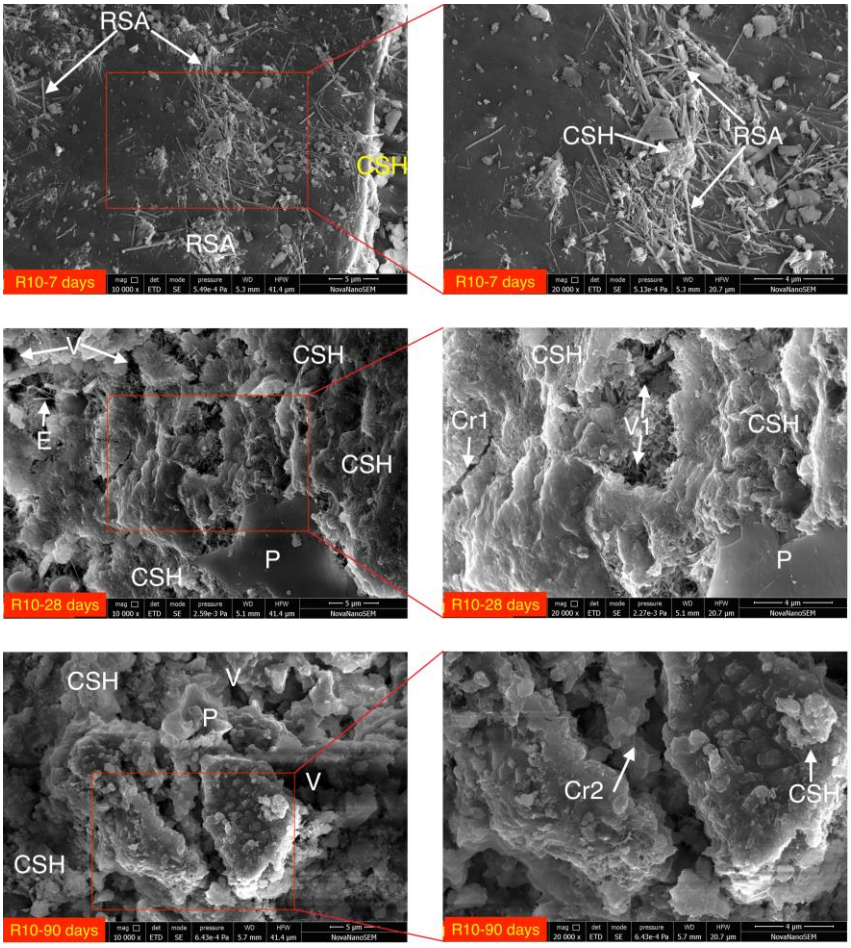

Figure 6.9 SEM micrograph of concrete of mix R10 at 7, 28 and 90 days of curing at 10,000 (left) and 20,000 (right) times magnification levels

(RSA - Rice Straw Ash; CSH - Calcium Silicate Hydrate; V - Void; E - Etrringite; P - Portlandite; Cr1 - micro-crack; Cr2 - microcrack being infilled; V1 - Void being infilled)

Figure 6.9 shows the SEM micrograph of the concrete of mix R10 (10% RSA) at 10,000 and 20,000 times magnification level. The addition of RSA reduced the amount of ettringite (E) in the concrete thereby reducing the potential damage to the concrete due to delayed ettringite formation (DEF) [294]. Few needle-shaped remnant RSA particles were observed in the SEM micrograph of R10 at 7 days of curing which signifies the potential of concrete admixed with RSA to develop strength even at late days of curing. The strength of mix R10 was more than the control mix R0 which can be associated with fewer amounts of voids (V). Some of these voids (V1) were being infilled with C-S-H gel at 28 days of curing which gives the indication that the additional C-S-H gel reduces the total volume of voids thereby increasing the compactness of the concrete matrix. Also, few microcracks were observed in mix R10 at 28 days and 90 days of curing. The microcrack in the hardened cementitious paste of concrete of mix R10 was being infilled (Cr2) with C-S-H gel at 90 days of curing while the microcrack at 28 days curing was not (Cr1). It demonstrated the positive impact of prolonged curing on the microstructure of concrete.

Figure 6.10 shows the SEM micrograph of the concrete of mix R10M5 (10% RSA + 5% MS) at 10,000 and 20,000 times magnification level. The number of voids in R10M5 were more than the number of voids (V) in other mixes of concrete admixed with combination of RSA and MS that is why R10M5 showed the least strength among these concrete mixes. However, they were lower than that in the mix R0 and R10 due to the presence of MS which is highly pozzolanic and has finer particles as compared to RSA. A microcrack was observed in the hardened cementitious paste only at 7 days of curing. Also, few unhydrated particles of MS were observed only at 7 days of curing. The absence of microcracks and unhydrated particles of MS at 28 and 90 days of curing give the indication that microstructure of admixed concrete was affected by MS mostly

at early days of curing [121]. Few unhydrated RSA particles were observed in concrete mix R10M5 while they were absent in the concrete mix R10 at 90 days of curing. It signifies that RSA was less effective in presence of MS.

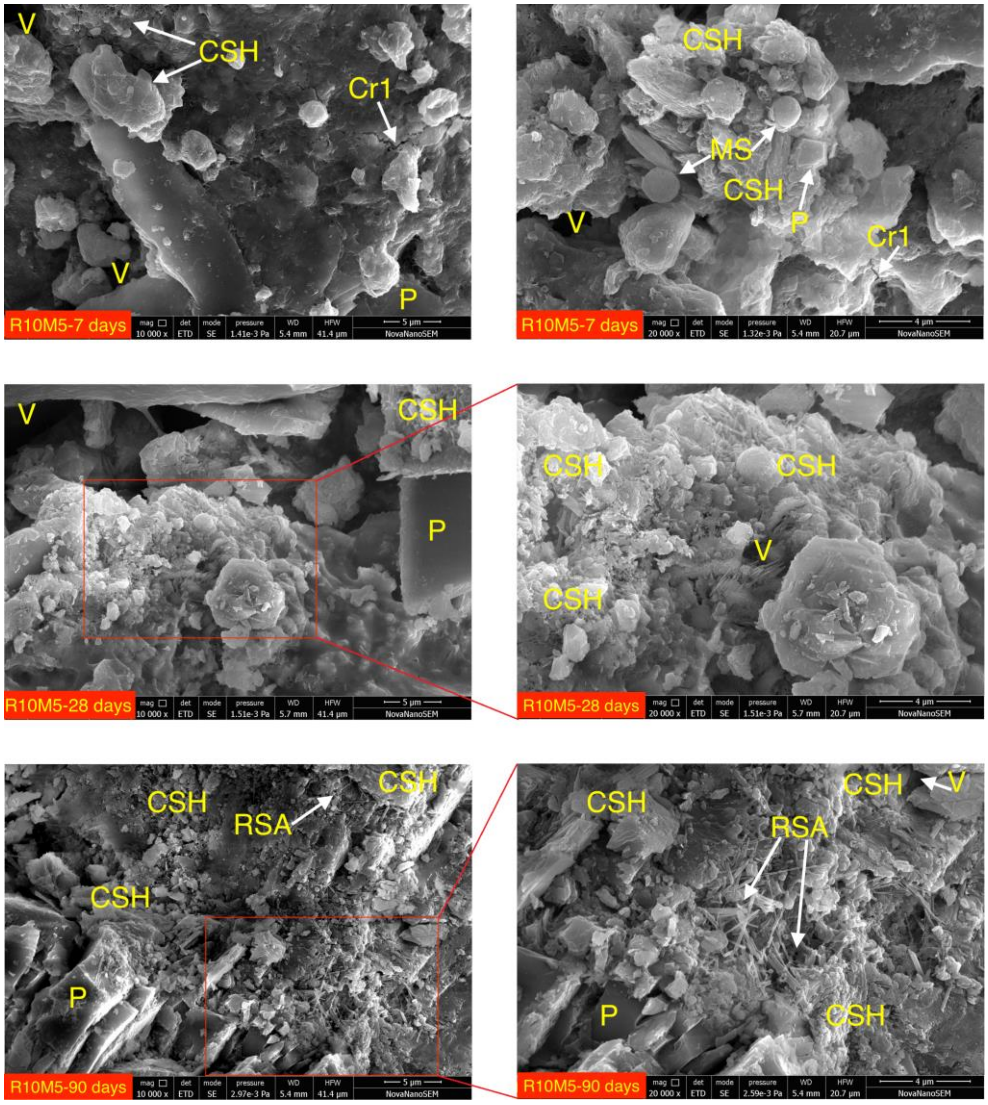

Figure 6.10 SEM micrograph of concrete of mix R10M5 at 7, 28 and 90 days of curing at 10,000 (left) and 20,000 (right) times magnification levels

(RSA - Rice Straw Ash; MS – Microsilica; CSH - Calcium Silicate Hydrate; V - Void; P - Portlandite; Cr1 - micro-crack)

Figure 6.11 shows the SEM micrograph of the concrete of mix R10M7.5 (10% RSA + 7.5% MS) at 10,000 and 20,000 times magnification level. The concrete mix R10M7.5 had more compact microstructure as compared to concrete mix R10 and R10M5. It gives the indication that the higher the amount of MS in concrete is (up to

7.5%), the better will be the microstructure of concrete. Few voids were observed at 7 days of curing but at later days of curing they were being infilled with additional C-S-H gel. Similarly, microcracks in the hardened cement paste at 90 days of curing were also being infilled with additional C-S-H gel. It can be concluded that consumption of portlandite ($Ca(OH)_2$) by pozzolanic action of RSA and MS strongly densifies the microstructure of concrete. Similar to the observations from micrograph of R10M5 (Figure 6.10), few unhydrated particles of MS were observed in mix R10M7.5 only at 7 days of curing.

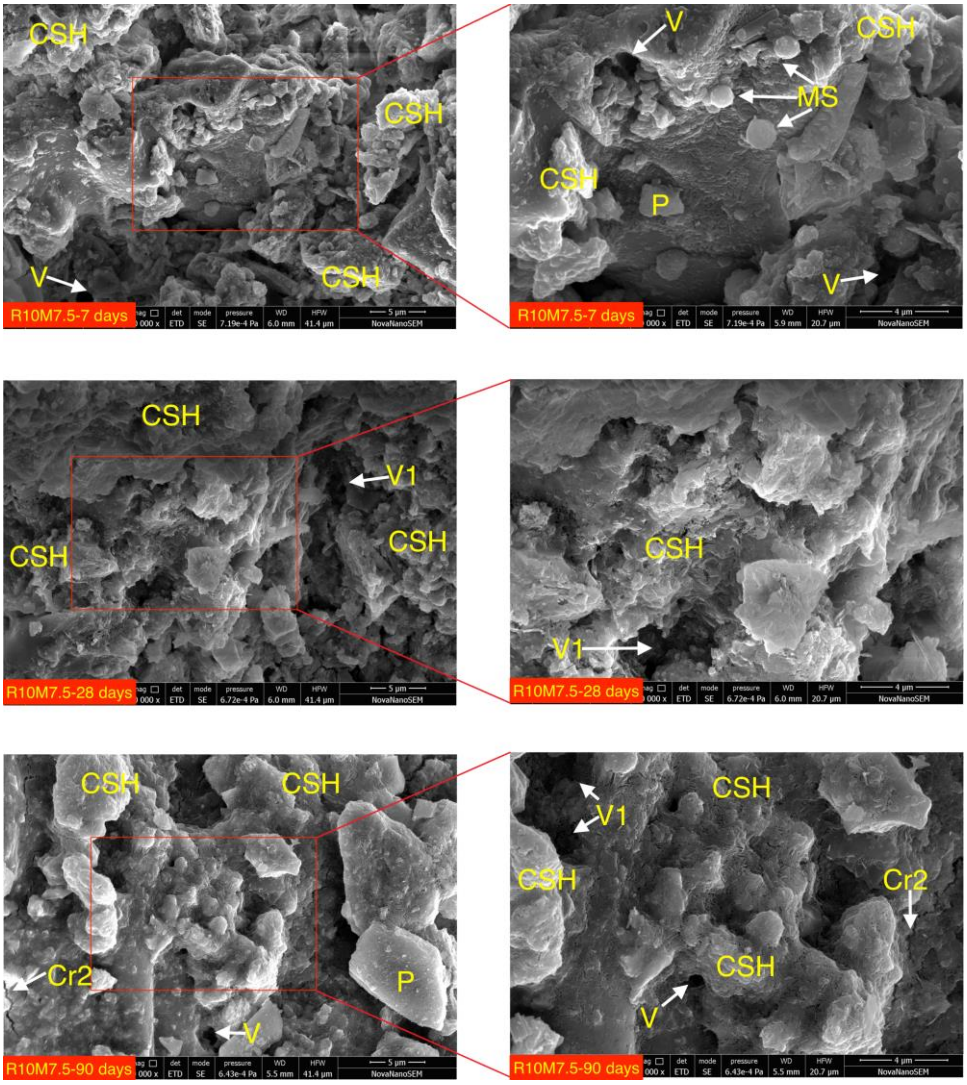

Figure 6.11 SEM micrograph of concrete of mix R10M7.5 at 7, 28 and 90 days of curing at 10,000 (left) and 20,000 (right) times magnification levels

(MS – Microsilica; CSH - Calcium Silicate Hydrate; V - Void; V1 – Void being infilled; P - Portlandite; Cr2 – microcrack being infilled)

Figure 6.12 shows the SEM micrograph of the concrete of mix R5M5 (5% RSA + 5% MS) at 10,000 and 20,000 times magnification level. The concrete of mix R5M5 had more compact microstructure as compared to concrete of mix R10M5 (Figure 6.10). It gives the indication that RSA doesn't densify the microstructure of concrete as much as MS does. It may be because of various reasons like coarser particles, higher water demand, lesser silica (SiO_2) content, presence of unburned carbon etc.

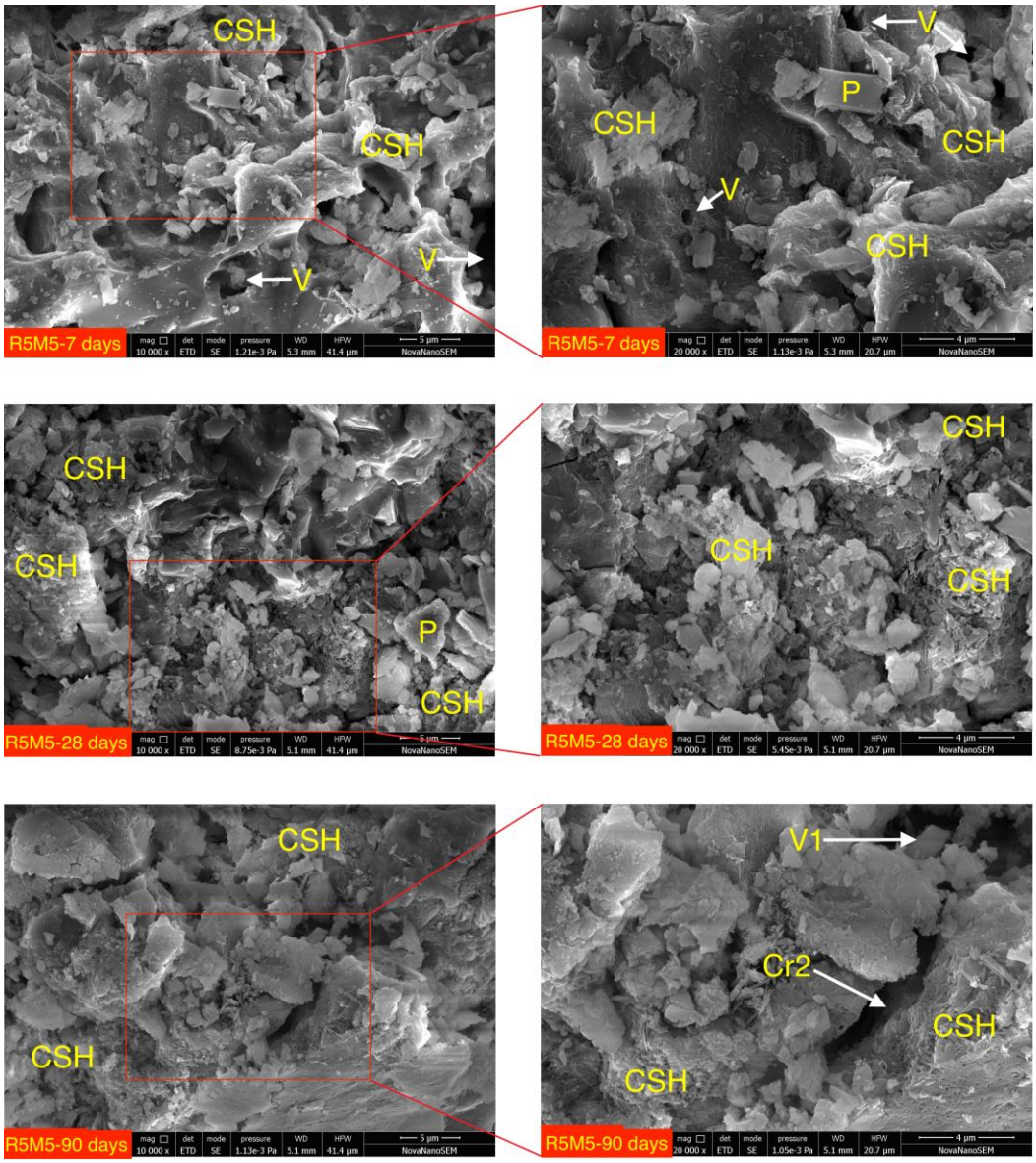

Figure 6.12 SEM micrograph of concrete of mix R5M5 at 7, 28 and 90 days of curing at 10,000 (left) and 20,000 (right) times magnification levels

(CSH - Calcium Silicate Hydrate; V - Void; V1 – Void being infilled; P - Portlandite; Cr2 – microcrack being infilled)

Figure 6.13 shows the SEM micrograph of the concrete of mix R5M7.5 (5% RSA + 7.5% MS) at 10,000 and 20,000 times magnification level. The micrograph of mix R5M7.5 justifies its maximum strength amongst the mixes studied by SEM analysis. It had least amount of voids, microcracks and portlandite content as compared to the other mixes at 7, 28 and 90 days of curing. Therefore it can be concluded that when RSA and MS were used together in the proportion of 5% and 7.5% respectively, the strength properties of the concrete improve significantly.

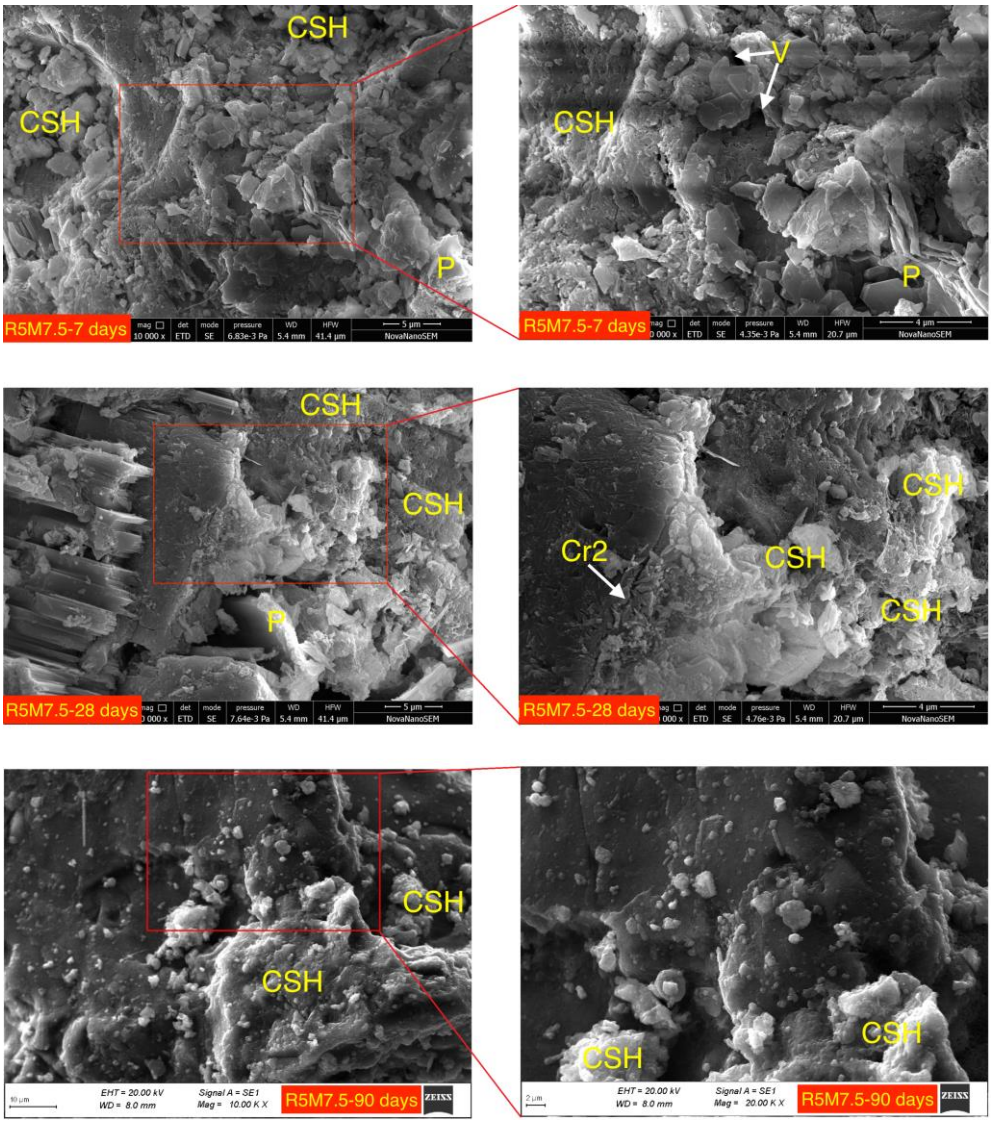

Figure 6.13 SEM micrograph of concrete of mix R5M7.5 at 7, 28 and 90 days of curing at 10,000 (left) and 20,000 (right) times magnification levels

(CSH - Calcium Silicate Hydrate; V - Void; P - Portlandite; Cr2 – microcrack being infilled)

6.8.2 Petrography Analysis

The petrographic examinations have been carried out for the six selected admixed concrete samples cured for 28 days. The photomicrographs of concrete samples R0, R10, R10M5, R10M7.5, R5M5 and R5M7.5 are shown in Figure 6.14, Figure 6.15, Figure 6.16, Figure 6.17, Figure 6.18 and Figure 6.19 respectively.

The photomicrographs of control mix R0 (Figure 6.14) show that it contains medium to coarse size quartz and feldspar grains and they were the main components of the groundmass. The amount of quartz grains were significantly more in comparison to the feldspar. Few grains of quartz and feldspar show corroded boundary due to the reaction between fine aggregates and cementing materials (Figure 6.14a). Few voids and microcracks were also observed in R0 (Figure 6.14a). The microcracks generally occur due to shrinkage of the hydrated cement paste [296]. The fracture in coarse aggregate was also observed which was being infilled with C-S-H gel (Figure 6.14a). These fractures may have occurred due to crushing, by nature or by other artificial means [297]. At few places, the groundmass was porous (Figure 6.14a and b). This could be one of the main reasons for lower strength of R0 as compared to other concrete mixes [215]. The presence of calcium hydroxide ($Ca(OH)_2$) gel was observed around the periphery of few quartz grains (Figure 6.14b). Portlandite ($Ca(OH)_2$) is considered to be the weakest hydration product because of its high solubility in water [298]. The concrete having high $Ca(OH)_2$ content is highly vulnerable to leaching and chemical attack [292]. One of the easiest ways to reduce the portlandite content in concrete is the addition of mineral admixtures.

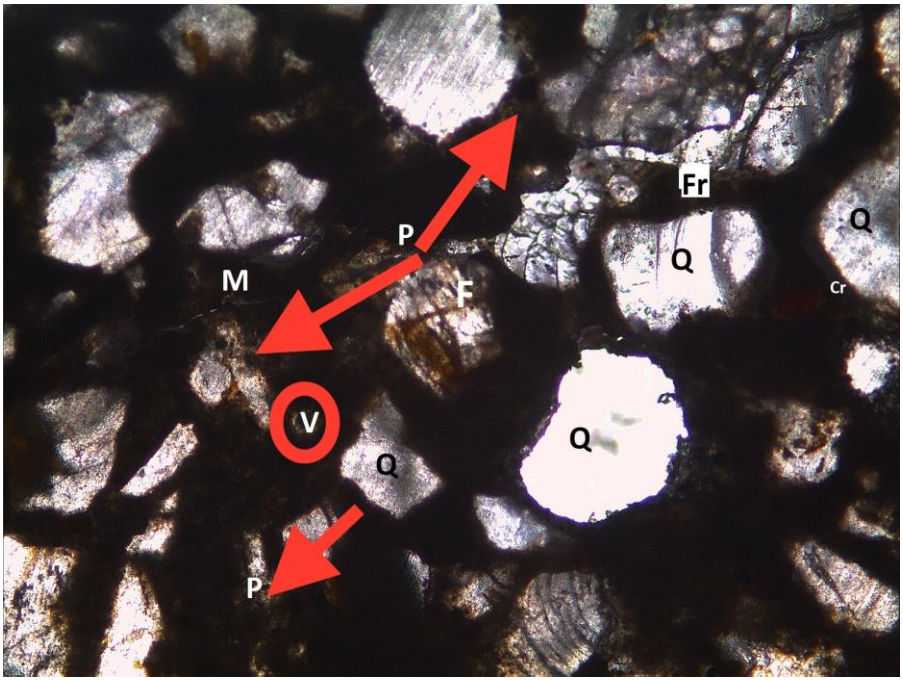

Figure 6.14 (a) Photomicrograph showing medium to small size voids (**'V'**). Also, noticed the porous (**'P'**) groundmass at few places. Coarse aggregate (**'CA'**) and mineral grains like quartz (**'Q'**) and K-feldspar (**'F'**) showing corroded boundary (**'Cr'**). Fracture (**'Fr'**) present in CA is being infilled. Microcracks (**'M'**) running across groundmass of hydrated cement paste. **[O.L. × 5x]**

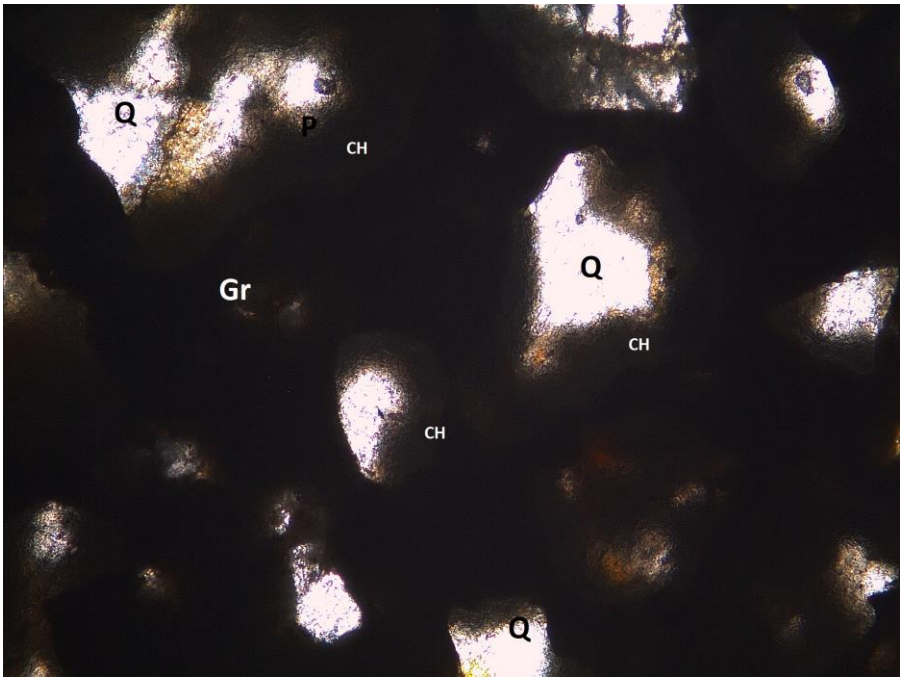

Figure 6.14 (b) Photomicrograph showing coating of calcium hydroxide gel (**'CH'**) around periphery of few mineral grains of Quartz (**'Q'**). Also, noticed the porous (**'P'**) groundmass and the presence of calcium hydroxide grains (**'Gr'**) within the groundmass. **[O.L. × 5x]**

Figure 6.14 Thin section photomicrographs of R0 after 28 days of water curing

The photomicrographs of concrete mix R10 (Figure 6.15) show that coarse aggregate and quartz grains show sharp contact with hydrated cement paste (Figure 6.15a). The addition of rice straw ash reduces the corrosion of aggregates. Fractures present in coarse aggregate were being infilled with cementitious materials (Figure 6.15a) and were considerably less in comparison to the control mix R0. Most of the voids were being infilled with additional C-S-H gel (grey to brown coloured rim around the voids) formed by the pozzolanic reaction of rice straw ash (Figure 6.15a and b). The formation of additional C-S-H gel reduces the size of the voids which may lead to improvement in the strength and durability properties [44]. The amount of $Ca(OH)_2$ was reduced significantly in concrete of mix R10 due to admixing of rice straw ash (Figure 6.15c). Thus it can be said that rice straw ash improves the performance of concrete against leaching and chemical attack. The Interfacial Transition Zone (ITZ) around the coarse aggregate was improved due to addition of rice straw ash (Figure 6.15c).

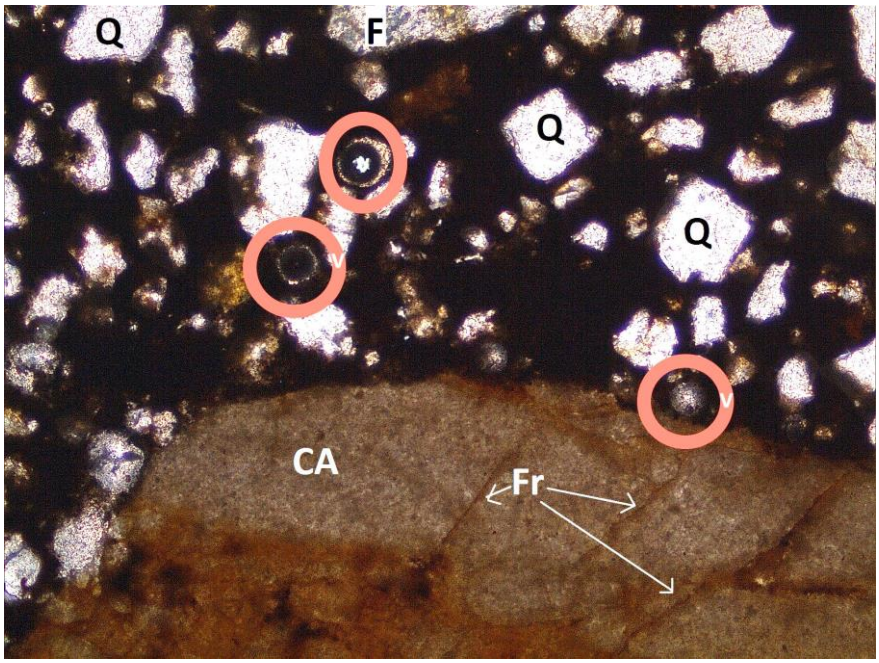

Figure 6.15 (a) Photomicrograph showing formation of rim around the voids (**'V'**) being infilled with cementitious material. Coarse aggregate (**'CA'**) and mineral grains like quartz (**'Q'**) and K-feldspar (**'F'**) showing sharp contact with the hydrated cementitious paste. Fractures (**'Fr'**) in coarse aggregate (**'CA'**) were being infilled with cementitious materials. **[O.L. × 2.5x]**

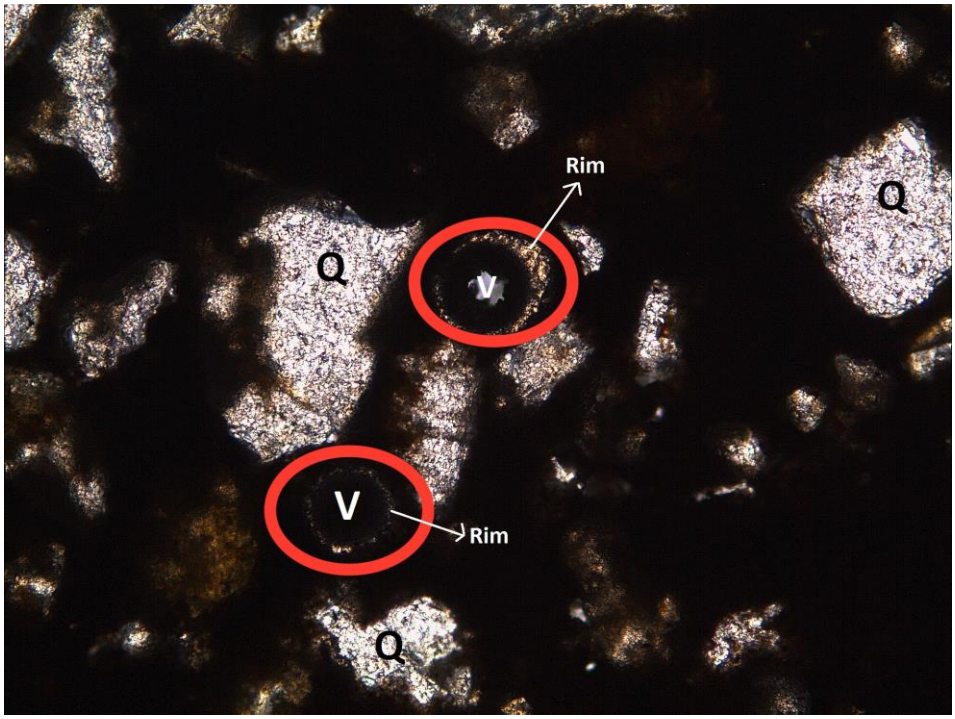

Figure 6.15 (b) Photomicrograph showing the formation of the C-S-H gel rim around the voids (**'V'**) being infilled with cementitious material. Quartz (**'Q'**) grains showing sharp contact with the hydrated cementitious paste. **[O.L. × 5x]**

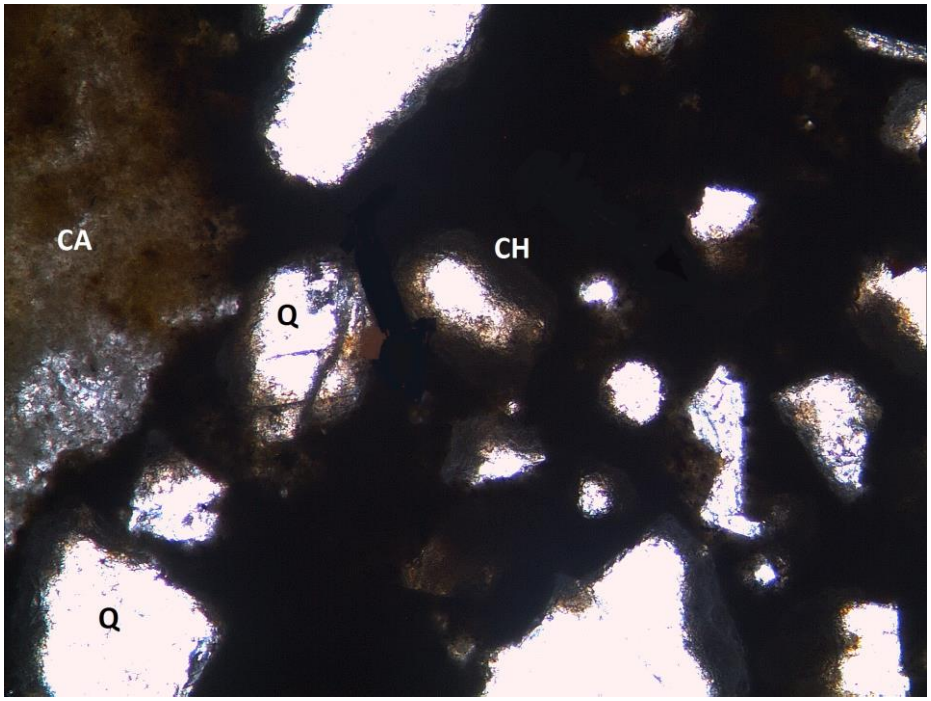

Figure 6.15 (c) Photomicrograph showing coating of calcium hydroxide (**'CH'**) gel around the periphery of the quartz (**'Q'**) grains. Improved interfacial transition zone around the perimeter of the coarse aggregate (**'CA'**). **[O.L. × 2.5x]**

Figure 6.15 Thin section photomicrographs of R10 after 28 days of water curing

The photomicrographs of mix R10M5 (Figure 6.16) show that all the microcracks (around the periphery of coarse aggregates) and voids (in the groundmass) were being infilled with C-S-H gel (Figure 6.16a, b and c) and were considerably reduced in comparison to the mix R0 and R10. It was most probably due to the consumption of $Ca(OH)_2$ by the combined pozzolanic action of microsilica and rice straw ash. The C-S-H gel rim formation around the voids depicts their infilling (Figure 6.16a). Quartz grains were the major components of the groundmass. The additional C-S-H gel was infilling the fractures present in the medium to coarse grained quartz (Figure 6.16c). The admixing of rice straw ash and microsilica prevented the corrosion of the aggregate and minerals. Ettringite particles in a void were also observed (Figure 6.16d). The remnant rice straw ash and microsilica particles within the groundmass (Figure 6.16b and c respectively) reveal that R10M5 will continue to develop strength even at late days of water curing (more than 28 days). In the SEM analysis of mix R10M5 (Figure 6.10), few remnant MS particles were observed at 7 days of curing while remnant RSA particles were observed even at 90 days of curing. Therefore it can be concluded from petrography and SEM analysis of mix R10M5 that MS was responsible for the strength up to 28 days of curing while RSA was mostly responsible for strength at later days of curing.

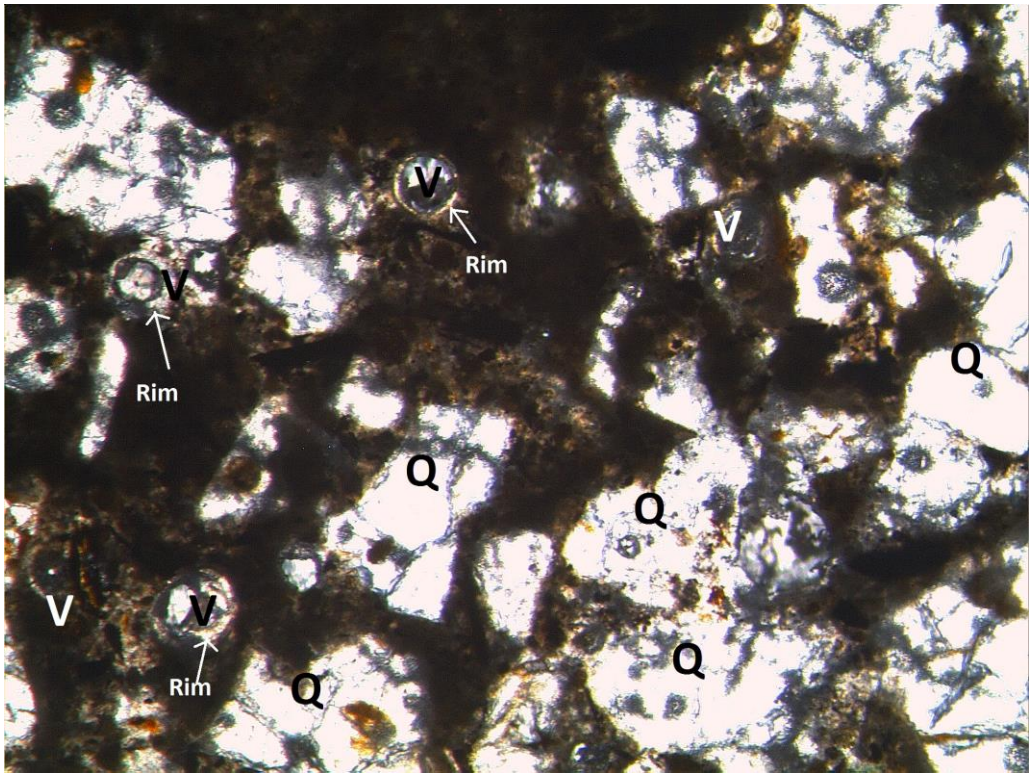

Figure 6.16 (a) Photomicrograph showing medium to small size voids (**'V'**) being infilled with cementitious paste. Medium to coarse-grained quartz (**'Q'**) and formation of C-S-H gel rim around few voids can be observed. **[O.L. × 5x]**

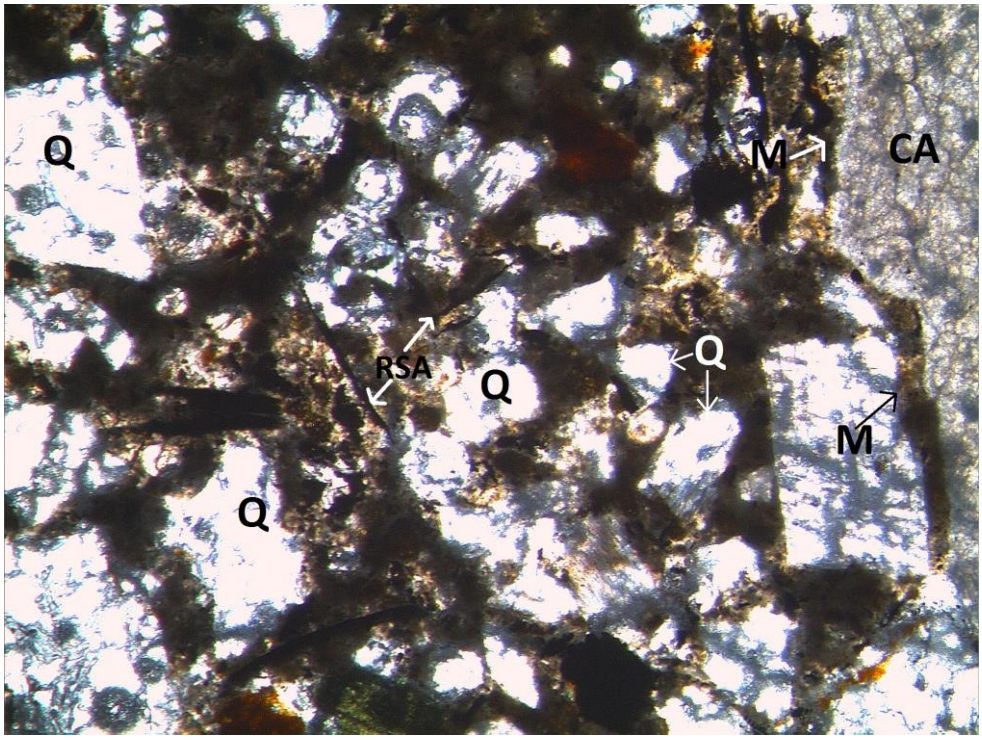

Figure 6.16 (b) Photomicrograph showing medium to coarse grained quartz (**'Q'**). Microcracks (**'M'**) along the periphery of coarse aggregate (**'CA'**) were being infilled with cementitious paste. Also, noticed the presence of undispersed needle-shaped rice straw ash (**'RSA'**) particles in the groundmass. **[O.L. × 5x]**

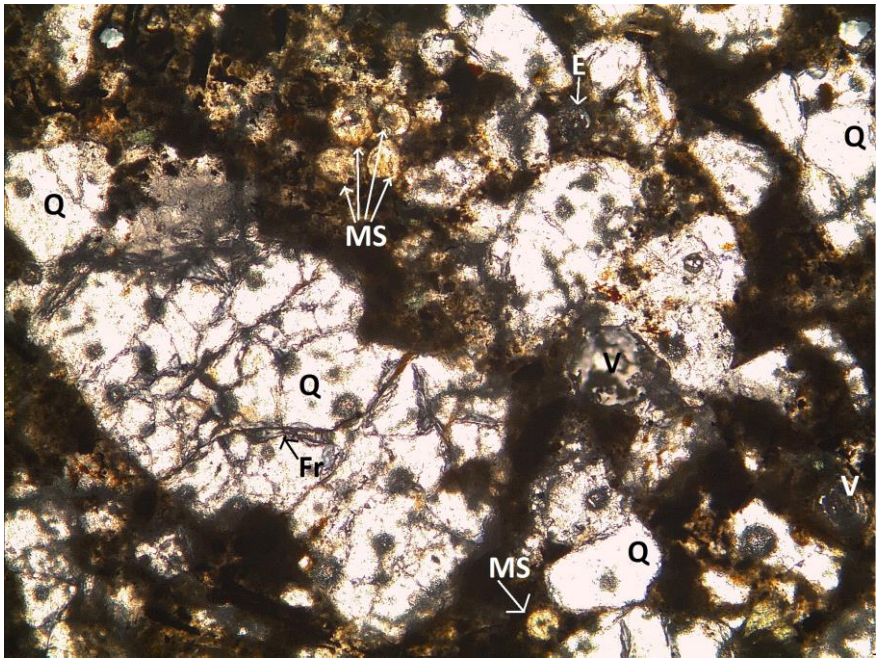

Figure 6.16 (c) Photomicrograph showing medium to coarse grained quartz (**'Q'**). Fractures (**'Fr'**) present within the quartz grains were being infilled with cementitious paste. Microsilica (**'MS'**) particles were also observed within the infilled voids. Also, noticed ettringite (**'E'**) in the void. **[O.L. × 5x]**

Figure 6.16 Thin section photomicrographs of R10M5 after 28 days of water curing

The photomicrographs of mix R10M7.5 (Figure 6.17) show fewer voids as compared to R0, R10 and R10M5 and all of them were partially infilled or completely infilled with cementitious gel (Figure 6.17a and b). Similar to R10M5, remnant microsilica particles in the infilled voids were also observed (Figure 6.17b and c). The microcracks generated due to the shrinkage of the hydrated cement paste were being infilled with additional C-S-H gel (Figure 6.17a). A layer of $Ca(OH)_2$ was observed around the periphery of some of the quartz grains (Figure 6.17a and b). The presence of $Ca(OH)_2$ as well as remnant microsilica particles within the infilled voids indicates that the formation of additional C-S-H gel by pozzolanic action of microsilica will take place even at later days of curing. The interfacial transition zone along the periphery of the coarse aggregate was dense (Figure 6.17c). Medium to coarse grained quartz and feldspar minerals were present within the groundmass with quartz being the dominating mineral.

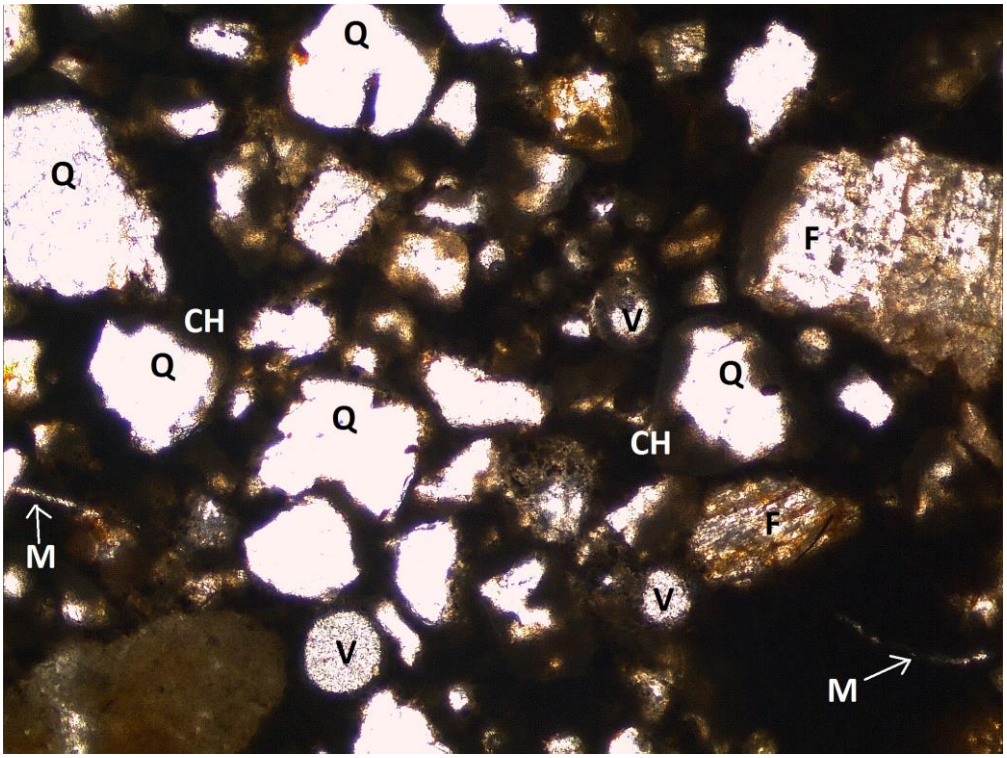

Figure 6.17 (a) Photomicrograph showing partially infilled voids (**'V'**). Medium to coarse grained quartz (**'Q'**) and K-feldspar (**'F'**) minerals were observed. Coating of calcium hydroxide gel (**'CH'**) around few quartz grains was seen. Microcracks (**'M'**) within the hydrated cementitious paste were being infilled with gels. **[O.L. × 2.5x]**

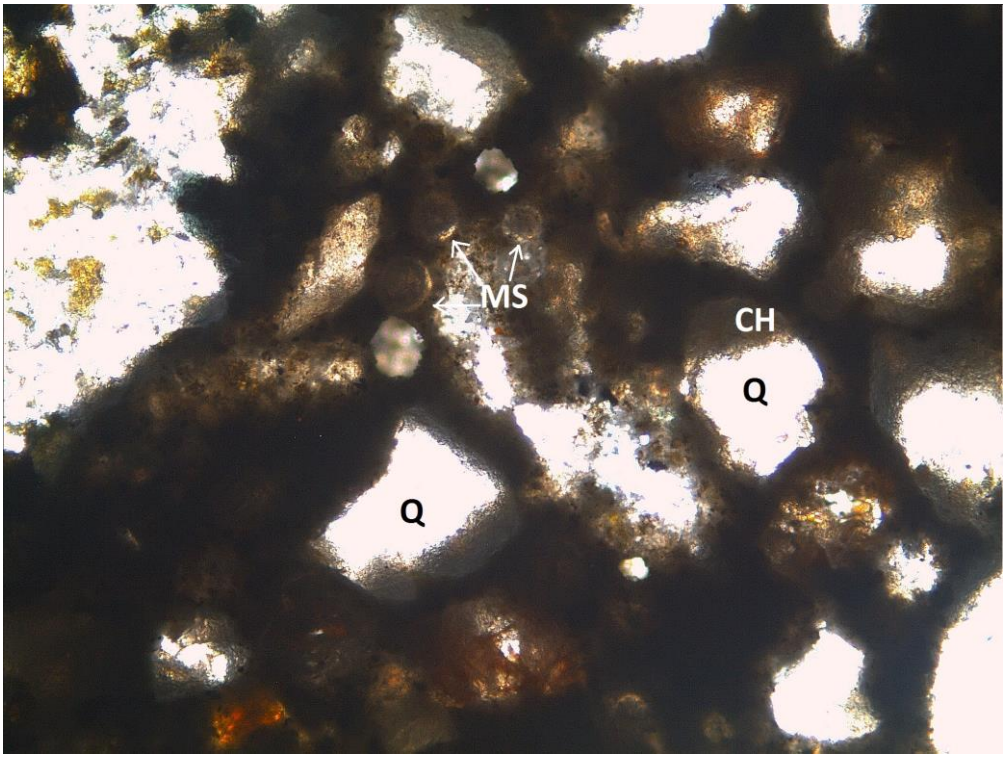

Figure 6.17 (b) Photomicrograph showing presence of undispersed microsilica (**'MS'**) particles within the infilled voids. Coating of calcium hydroxide gel (**'CH'**) around few quartz grains was observed. **[O.L. × 5x]**

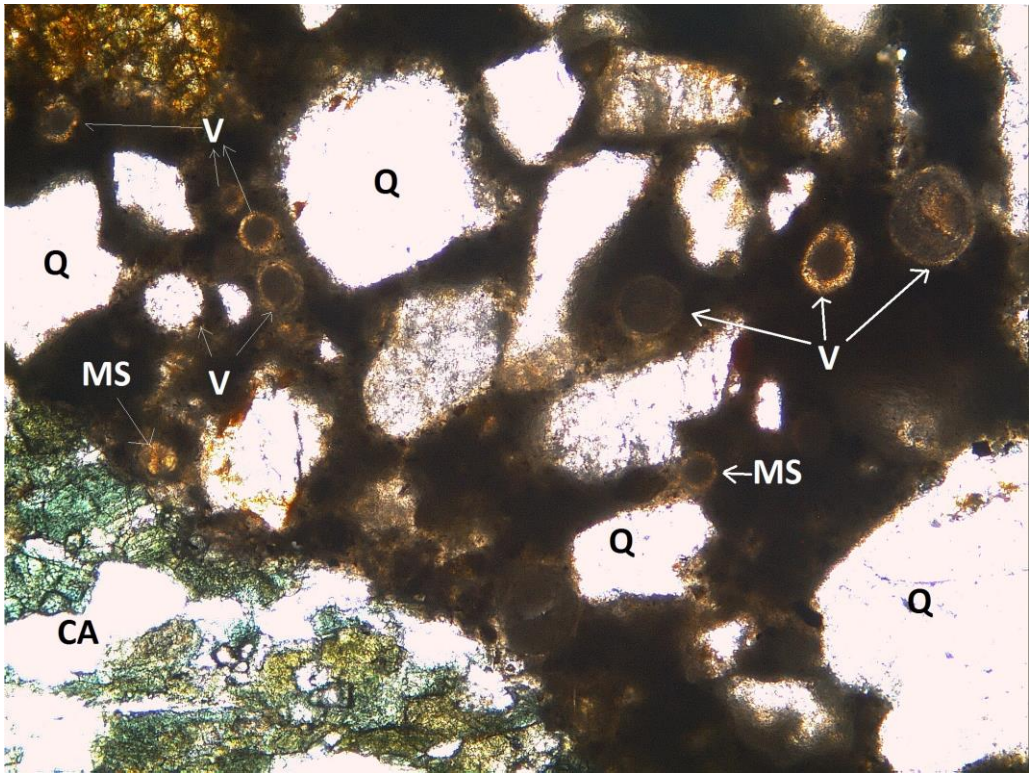

Figure 6.17 (c) Photomicrograph showing medium to coarse grained quartz (**'Q'**) minerals. Few undispersed microsilica (**'MS'**) particles within the partially infilled voids were observed along with completely filled voids (**'V'**). Interfacial transition zone around the periphery of coarse aggregate (**'CA'**) was dense. Also, noticed the rim around the partially infilled voids. **[O.L. × 5x]**

Figure 6.17 Thin section photomicrographs of R10M7.5 after 28 days of water curing

The photomicrographs of mix R5M5 (Figure 6.18) show infilling of voids by remnant rice straw ash and microsilica particles (Figure 6.18a and b). Few rice straw ash particles were also found in the groundmass (Figure 6.18c). Medium to coarse grained quartz minerals were the major constituents of the groundmass (Figure 6.18a, b and c). The coating of $Ca(OH)_2$ around the quartz grains was also seen (Figure 6.18b and d). Most probably, this coating of portlandite could have been consumed by the pozzolanic action of remnant rice straw ash and microsilica particles at later days of moist curing. The ITZ had improved significantly therefore the coarse aggregates show sharp contact with the cementitious paste (Figure 6.18a). Few microcracks and voids were fully infilled with additional C-S-H gel (Figure 6.18d).

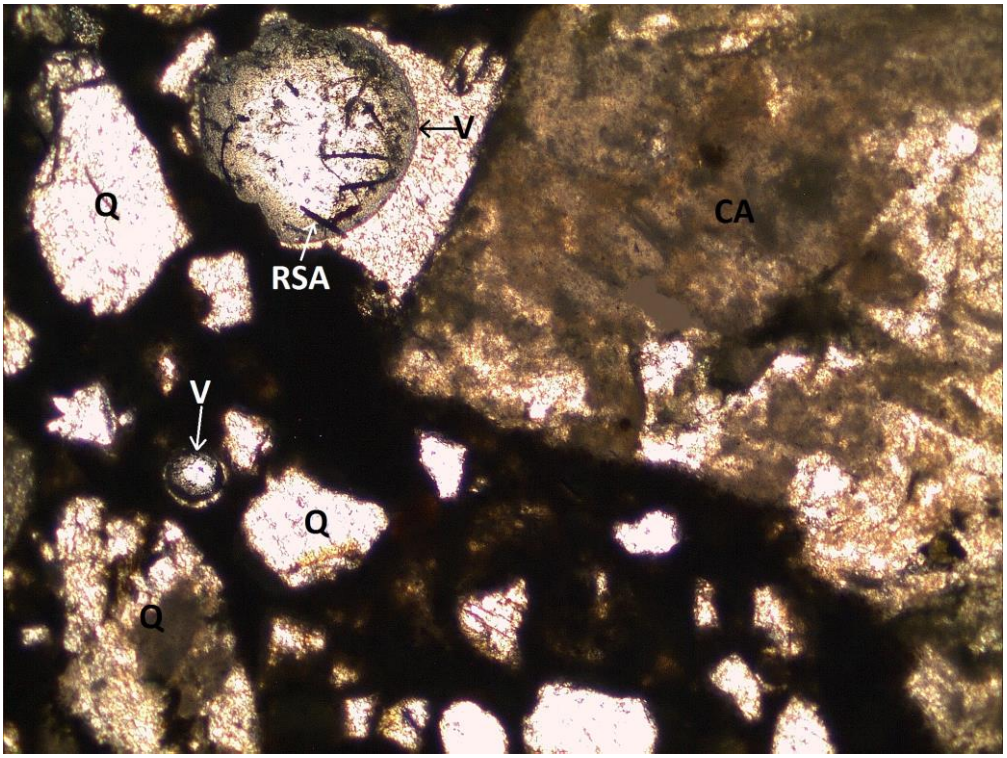

Figure 6.18 (a) Photomicrograph showing the infilled void (**'V'**) with needle-shaped rice straw ash particles (**'RSA'**) and cementitious paste. Few quartz (**'Q'**) grains as well as coarse aggregate (**'CA'**) show sharp contact with the groundmass. **[O.L. × 2.5x]**

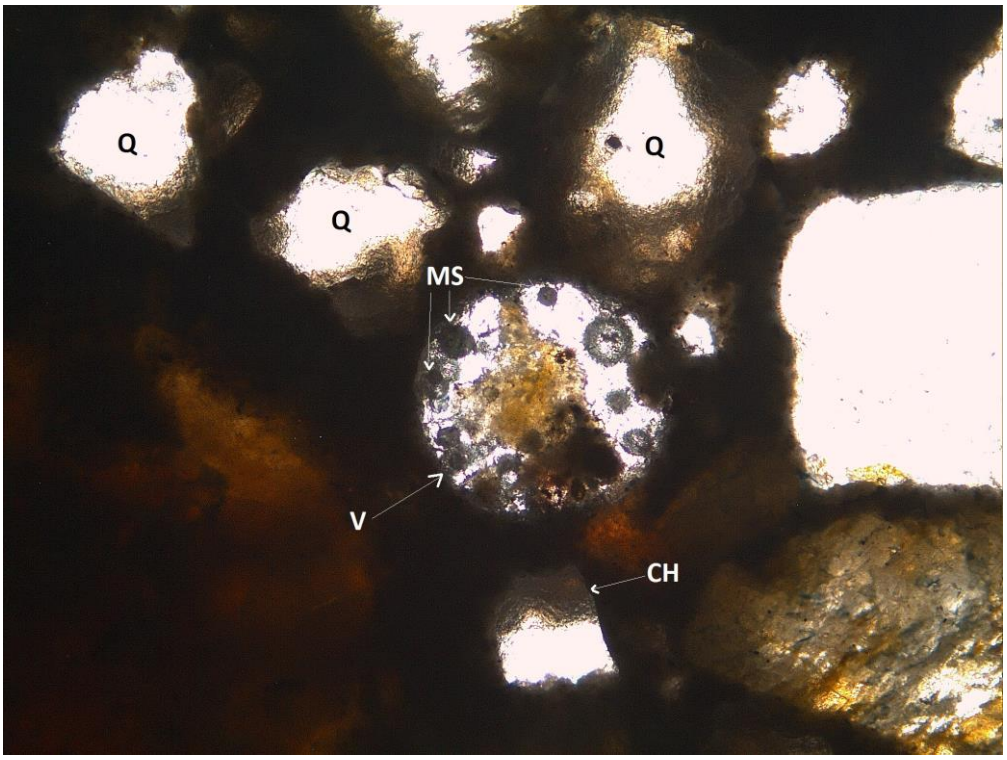

Figure 6.18 (b) Photomicrograph showing coating of calcium hydroxide (**'CH'**) gel around periphery of medium size quartz (**'Q'**) grains. Large size void (**'V'**) was partially infilled with hydrated cementitious paste and undispersed microsilica (**'MS'**) particles. **[O.L. × 5x]**

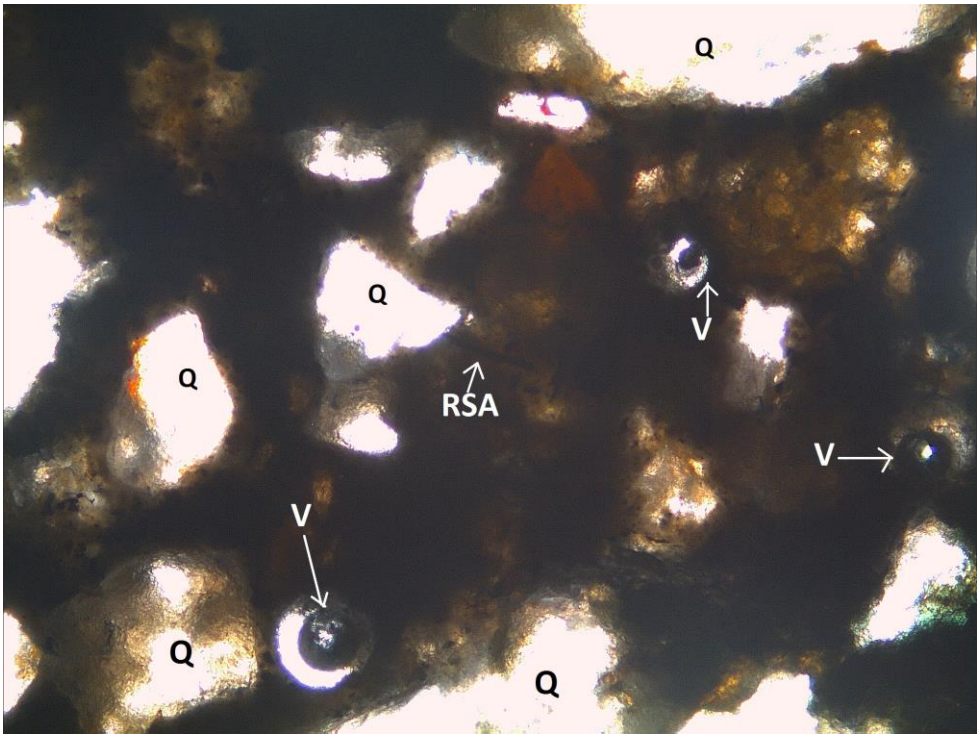

Figure 6.18 (c) Photomicrograph showing remnant needle-shaped rice straw ash particles (**'RSA'**) in the groundmass. Medium to coarse-grained quartz (**'Q'**) mineral can also be seen. Also noticed partially infilling of voids (**'V'**). **[O.L. × 5x]**

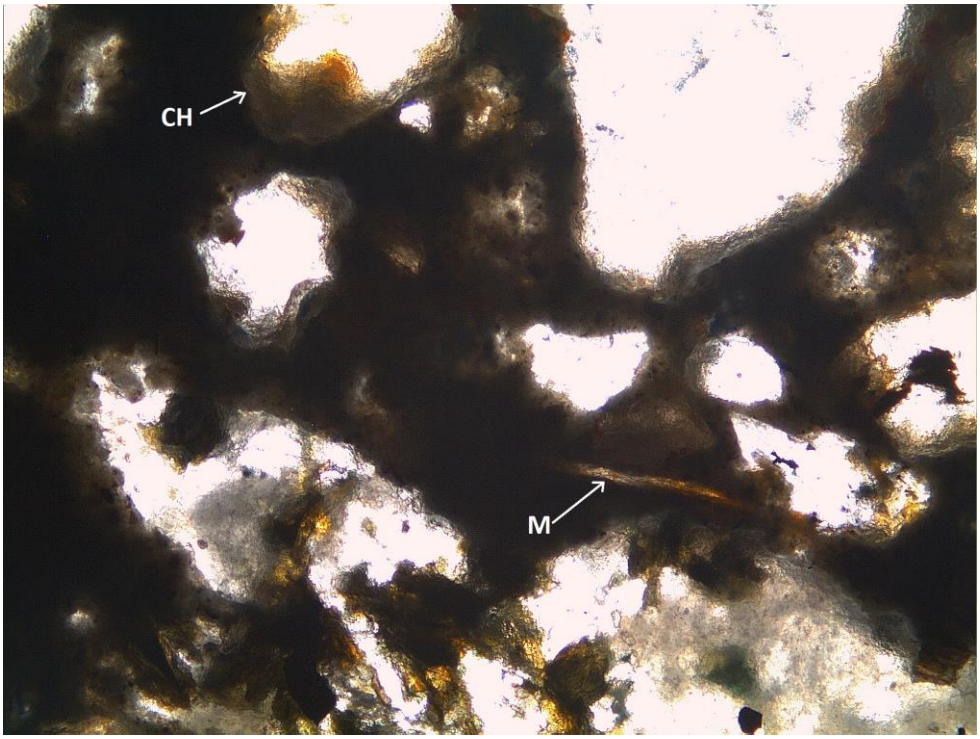

Figure 6.18 (d) Photomicrograph showing infilled microcrack (**'M'**) present in the groundmass. Also noticed coating of calcium hydroxide (**'CH'**) gel around quartz grain. **[O.L. × 5x]**

Figure 6.18 Thin section photomicrographs of R5M5 after 28 days of water curing

The photomicrographs of mix R5M7.5 (Figure 6.19) show the formation of rim of C-S-H gel around some of the voids (Figure 6.19a, b and c). At few places, medium to coarse grained quartz minerals and coarse aggregates show sharp contact with the cementitious groundmass (Figure 6.19c and d). The ITZ around the coarse aggregates was dense (Figure 6.19c). Microcracks were not found in this sample. The remnant rice straw ash and microsilica particles were also observed (Figure 6.19b and c). Few voids were partially infilled with C-S-H gel (Figure 6.19a and b) while some were fully infilled with cementitious paste (Figure 6.19c and d). Partially as well as fully infilled voids and the absence of microcracks were the main reason behind the maximum strength of R5M7.5 in comparison with other mixes which were analysed by petrography. Brown coloured iron oxide was also observed only in concrete of mix R5M7.5 (Figure 6.19d).

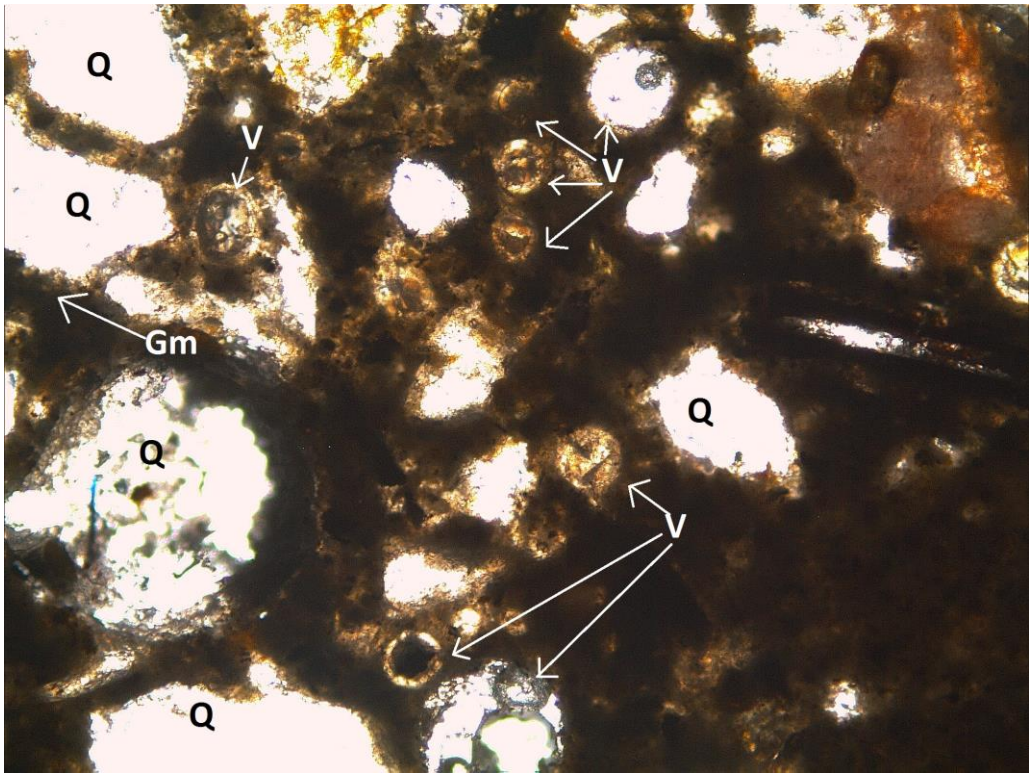

Figure 6.19 (a) Photomicrograph showing medium to coarse grained quartz (**'Q'**) mineral. Very thin rim around partially infilled voids (**'V'**) were observed. **[O.L. × 5x]**

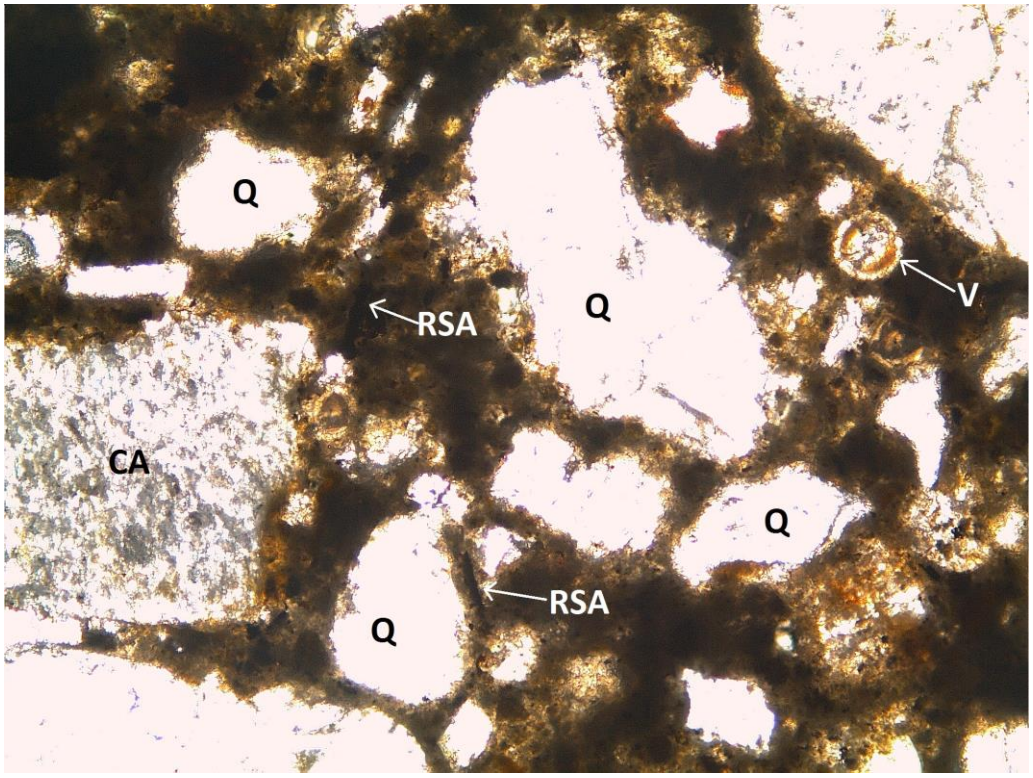

Figure 6.19 (b) Photomicrograph showing remnant needle-shaped rice straw ash particles (**'RSA'**) within the groundmass. Medium to coarse grained quartz (**'Q'**) minerals were present within the groundmass. Voids (**'V'**) were partially infilled with cementitious paste. Rim around the voids were also present. **[O.L. × 5x]**

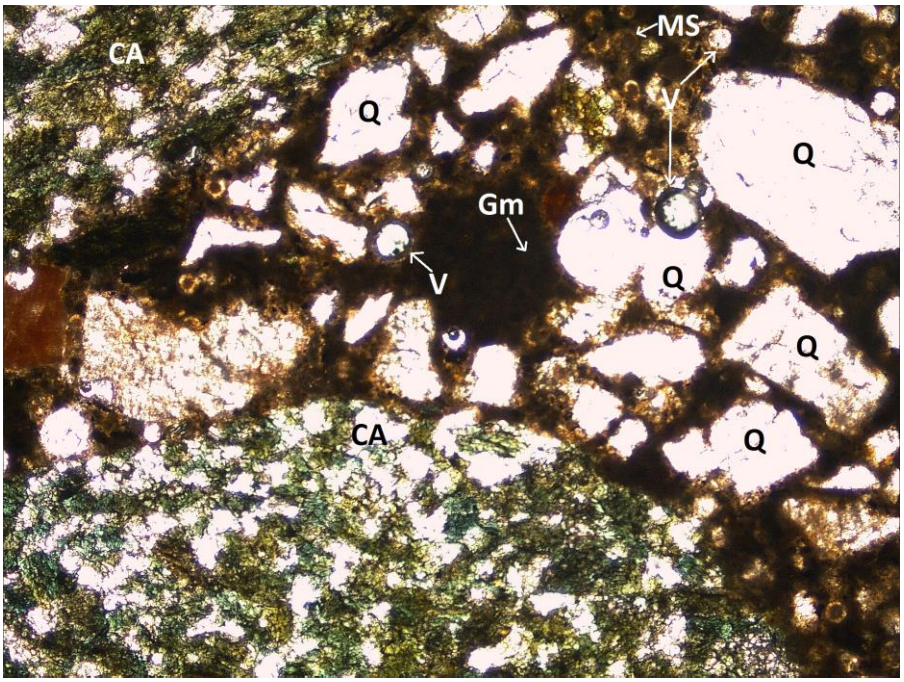

Figure 6.19 (c) Photomicrograph showing infilled rim occurring around the voids (**'V'**) with cementitious paste. Few quartz (**'Q'**) grains were observed. Undispersed microsilica (**'MS'**) particles within the infilled voids and cementitious groundmass (**'Gm'**) were also seen. Interfacial transition zone along the coarse aggregate (**'CA'**) was sharp. **[O.L. × 2.5x]**

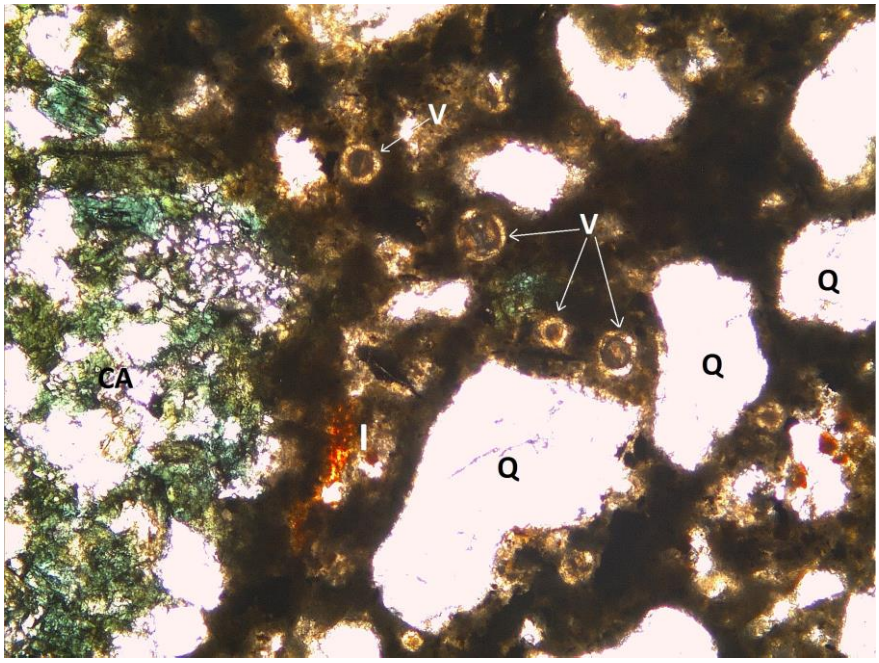

Figure 6.19 (d) Photomicrograph showing medium to small size voids (**'V'**) being partially and fully infilled with cementitious material. Quartz (**'Q'**) grains were also present in the groundmass. At few places, coarse aggregate (**'CA'**) shows sharp contact with the cementitious groundmass. Formation of Iron Oxide can also be seen (**'I'**). **[O.L. X 5x]**

Figure 6.19 Thin section photomicrographs of R5M7.5 after 28 days of water curing

The addition of RSA and MS reduces the microcracks considerably w.r.t. control mix R0 due to their pozzolanic action in which they consume most of the $Ca(OH)_2$ to produce additional C-S-H gel. The addition of these mineral admixtures has also decreased the corrosion of aggregates which can be associated with improved durability and strength properties of concrete. It can be perceived from the presence of remnant RSA and MS particles that the strength of the admixed concrete will continue to grow even at later days of water curing. The ITZ also improved drastically in the admixed concrete. The shape of the quartz grains was mostly anhedral or subhedral.

6.9 PREDICTION MODELS

Various equations between different parameters were developed by regression analysis from ORIGIN 2019 software based on the findings of experimental studies.

These equations will help in anticipating one parameter from another without gathering complete information. Although predicting future results is necessarily questionable, so exact data about what's to come is much of the time incomprehensible. But the forecast can be helpful in making arrangements about conceivable developments.

6.9.1 Relationship between Mechanical Strength and Curing Age

Different strengths (compressive or flexural or split tensile) of concrete of various mixes were dependent on the age of curing. Therefore, the mathematical relationship between them was described by logarithmic equation in the form of Equation 6.1 with a high coefficient of determination.

$$f(x) = a + b \times \ln(x + c) \qquad 6.1$$

where, f(x) = strength (compressive/flexural/split tensile) of concrete (MPa),
a, b, c = constants,
x = curing age (days)

The logarithmic equations between strength (compressive, flexural and split tensile) and curing age are given in Table 6.9, 6.10 and 6.11 respectively. These equations were derived from the experimental data given in Table 6.3, 6.5 and 6.7 respectively. It is clearly visible that the equation for compressive strength of mix R10M7.5 (Table 6.9), flexural strength of mix M7.5 (Table 6.10) and split tensile strength of mix R5M7.5 (Table 6.11) had the highest coefficient of determination (R^2=0.9494, 0.9773 and 0.9461 respectively). It means that 94.94% of the variance in compressive strength of mix R10M7.5, 97.73% of the variance in flexural strength of mix M7.5 and 94.61% of the variance in split tensile strength of mix R5M7.5 is described by their curing age. Based on this observation, it can be concluded that the compressive strength of mix R10M7.5, flexural strength of mix M7.5 and split tensile

strength of mix R5M7.5 could be predicted more accurately from curing age as compared to other mixes.

Table 6.9 Prediction models for compressive strength ('f_c') w.r.t. curing age ('x')

Mix	Prediction Models	R^2	Validity
R0	$f_c = 34.74 + 3.68 \times \ln(x - 2.86)$	0.9398	$365 \geq x > 2.86$
R10	$f_c = 34.77 + 3.75 \times \ln(x - 2.86)$	0.9434	$365 \geq x > 2.86$
M2.5	$f_c = 36.16 + 4.05 \times \ln(x - 2.87)$	0.9241	$365 \geq x > 2.87$
M5	$f_c = 36.95 + 4.09 \times \ln(x - 2.87)$	0.9244	$365 \geq x > 2.87$
M7.5	$f_c = 37.57 + 4.10 \times \ln(x - 2.88)$	0.9177	$365 \geq x > 2.88$
M10	$f_c = 30.21 + 5.14 \times \ln(x - 2.57)$	0.9071	$365 \geq x > 2.57$
R5M5	$f_c = 35.43 + 3.90 \times \ln(x - 2.86)$	0.9435	$365 \geq x > 2.86$
R5M7.5	$f_c = 36.91 + 3.99 \times \ln(x - 2.88)$	0.9251	$365 \geq x > 2.88$
R10M5	$f_c = 35.08 + 3.80 \times \ln(x - 2.86)$	0.9455	$365 \geq x > 2.86$
R10M7.5	$f_c = 34.96 + 3.89 \times \ln(x - 2.85)$	0.9494	$365 \geq x > 2.85$

Table 6.10 Prediction models for flexural strength ('f_r') w.r.t. curing age ('x')

Mix	Prediction Models	R^2	Validity
R0	$f_r = 4.39 + 0.40 \times \ln(x - 2.64)$	0.9489	$365 \geq x > 2.64$
R10	$f_r = 4.48 + 0.39 \times \ln(x - 2.70)$	0.9519	$365 \geq x > 2.70$
M2.5	$f_r = 4.76 + 0.39 \times \ln(x - 2.62)$	0.9504	$365 \geq x > 2.61$
M5	$f_r = 5.50 + 0.26 \times \ln(x - 2.86)$	0.9666	$365 \geq x > 2.86$
M7.5	$f_r = 5.77 + 0.22 \times \ln(x - 2.95)$	0.9773	$365 \geq x > 2.95$
M10	$f_r = 4.13 + 0.51 \times \ln(x - 2.45)$	0.9378	$365 \geq x > 2.45$
R5M5	$f_r = 4.64 + 0.39 \times \ln(x - 2.59)$	0.9475	$365 \geq x > 2.59$
R5M7.5	$f_r = 5.35 + 0.27 \times \ln(x - 2.86)$	0.9606	$365 \geq x > 2.86$
R10M5	$f_r = 4.50 + 0.40 \times \ln(x - 2.64)$	0.9505	$365 \geq x > 2.64$
R10M7.5	$f_r = 4.53 + 0.40 \times \ln(x - 2.52)$	0.9456	$365 \geq x > 2.52$

Table 6.11 Prediction models for split tensile strength ('f_t') w.r.t. curing age ('x')

Mix	Prediction Models	R^2	Validity
R0	$f_t = 2.78 + 0.29 \times \ln(x - 2.83)$	0.9457	$365 \geq x > 2.83$
R10	$f_t = 2.82 + 0.29 \times \ln(x - 2.84)$	0.9348	$365 \geq x > 2.84$
M2.5	$f_t = 2.99 + 0.31 \times \ln(x - 2.77)$	0.9324	$365 \geq x > 2.77$
M5	$f_t = 3.25 + 0.33 \times \ln(x - 2.67)$	0.9276	$365 \geq x > 2.67$
M7.5	$f_t = 3.48 + 0.34 \times \ln(x - 2.58)$	0.9180	$365 \geq x > 2.58$
M10	$f_t = 2.89 + 0.38 \times \ln(x - 2.68)$	0.9245	$365 \geq x > 2.68$
R5M5	$f_t = 2.91 + 0.29 \times \ln(x - 2.59)$	0.9460	$365 \geq x > 2.59$
R5M7.5	$f_t = 3.10 + 0.35 \times \ln(x - 2.51)$	0.9461	$365 \geq x > 2.51$
R10M5	$f_t = 2.84 + 0.30 \times \ln(x - 2.82)$	0.9342	$365 \geq x > 2.82$
R10M7.5	$f_t = 2.85 + 0.30 \times \ln(x - 2.81)$	0.9380	$365 \geq x > 2.81$

6.9.2 Relationship between Compressive and Flexural Strength

Figure 6.20 shows the relationship between the experimental compressive strength of each mix and their corresponding experimental flexural strength at each curing age. As a result of this, two equations as shown in Equation 6.2 (a) and (b) were obtained. It is observed that the coefficient of determination of Equation 6.2(a) is higher than that of Equation 6.2(b). However, various standards use the format of Equation 6.2(b). While discussing within the framework of the Indian Standard (IS 456:2000) [270], it is observed that the multiplying constant has a higher value of 0.87 for RSA and MS admixed concrete as compared to 0.70 for conventional OPC concrete.

$$f_r = 0.561 \times f_c^{0.615} \qquad R^2 = 0.9076 \qquad 6.2\ (a)$$

$$f_r = 0.87 \times \sqrt{f_c} \qquad R^2 = 0.88 \qquad 6.2\ (b)$$

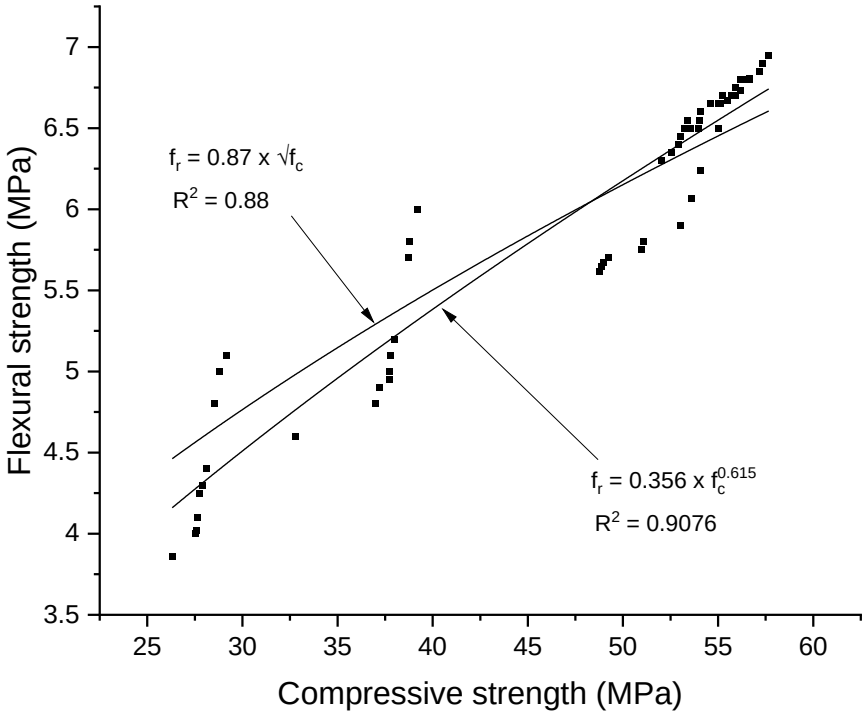

Figure 6.20 Comparison between compressive strength (f_c) and flexural strength (f_r)

In order to make a comparison between various standards dealing with conversion of characteristic compressive strength to characteristic flexural strength (f_r),

relationship as shown in Table 6.12 becomes useful. It may be noted that few standards stipulate evaluation of characteristic compressive strength (f_{cc}) based on the cylindrical specimen (15 cm dia. and 30 cm height). Suggestions made by several past studies indicate a factor of 0.80 for its conversion to cube compressive strength (150 mm size) [299]–[303].

Table 6.12 Empirical relationships between characteristic compressive and flexural strength [304]

Specifications	Country	Empirical Expression	Equation No.
Canadian Code of Practice [305]	Canada	$f_r = 0.60 \times \sqrt{f_{cc}}$	6.3[a]
BS-8110	Britain	$f_r = 0.60 \times \sqrt{f_{cc}}$	6.4[a]
EC-02	Europe	$f_r = 0.20 \times \sqrt{f_c}$	6.5
NZS-3101	New Zealand	$f_r = 0.60 \times \sqrt{f_{cc}}$	6.6[a]
ACI	USA	$f_r = 0.62 \times \sqrt{f_{cc}}$	6.7
IS 456 : 2000	India	$f_r = 0.70 \times \sqrt{f_c}$	6.8

[a]Equation 6.3, 6.4 and 6.6 have the same empirical expression

Table 6.13 compares the 28 days flexural strength of RSA and MS admixed concrete obtained through experiment with that derived through Equations 6.2(a) and (b) and equations given in Table 6.12. It can be observed that both Equations 6.2(a) and (b) provided predicted flexural strength values more accurately to experimental flexural strength (with ratio close to 1) as compared to other equations whose results were either too high or too low from the experimental observations. On comparing flexural strength obtained from Equation 6.2(a) and (b), it can be observed that Equation 6.2(b) (with lower coefficient of determination) gave marginally better results as compared to Equation 6.2(a). Therefore, it can be said with certainty that for predicting flexural strength of RSA and MS admixed concrete from respective compressive strength, Equation 6.2(a) will be more accurate for curing age of 3, 7, 60, 90 and 365 days while Equation 6.2(b) will be more accurate for curing age of 28 days.

Table 6.13 Comparison of different characteristic compressive-flexural strength equations

Mix	Experimental Strength (MPa)			Predicted Flexural Strength (MPa) from Equations						Ratio of Experimental & Predicted Flexural Strength					
	f_c	f_{cc}=0.8 × f_c	f_r	6.2 (a)	6.2 (b)	6.3	6.5	6.7	6.8	$\frac{f_r}{6.2(a)}$	$\frac{f_r}{6.2(b)}$	$\frac{f_r}{6.3}$	$\frac{f_r}{6.5}$	$\frac{f_r}{6.7}$	$\frac{f_r}{6.8}$
R0	48.77	39.01	5.62	6.13	6.08	3.75	9.80	3.87	4.89	0.92	0.93	1.50	0.57	1.45	1.15
R10	48.88	39.10	5.65	6.13	6.08	3.75	9.82	3.88	4.89	0.92	0.93	1.51	0.58	1.46	1.16
M2.5	53.02	42.42	5.9	6.45	6.33	3.91	10.66	4.04	5.10	0.91	0.93	1.51	0.55	1.46	1.16
M5	54.08	43.26	6.24	6.53	6.40	3.95	10.87	4.08	5.15	0.96	0.98	1.58	0.57	1.53	1.21
M7.5	55.01	44.00	6.5	6.60	6.45	3.98	11.06	4.11	5.19	0.99	1.01	1.63	0.59	1.58	1.25
M10	51.07	40.86	5.8	6.30	6.22	3.84	10.27	3.96	5.00	0.92	0.93	1.51	0.56	1.46	1.16
R5M5	50.96	40.77	5.75	6.29	6.21	3.83	10.24	3.96	5.00	0.91	0.93	1.50	0.56	1.45	1.15
R5M7.5	53.61	42.89	6.07	6.49	6.37	3.93	10.78	4.06	5.13	0.93	0.95	1.54	0.56	1.50	1.18
R10M5	48.99	39.20	5.67	6.14	6.09	3.76	9.85	3.88	4.90	0.92	0.93	1.51	0.58	1.46	1.16
R10M7.5	49.22	39.38	5.7	6.16	6.10	3.77	9.89	3.89	4.91	0.93	0.93	1.51	0.58	1.47	1.16

6.9.3 Relationship between Compressive and Split Tensile Strength

Figure 6.21 shows the relationship between the experimental compressive strength of each mix and their corresponding experimental split tensile strength at each curing age. As a result of this, two equations as shown in Equation 6.9 (a) and (b) were obtained. It is observed that the coefficient of determination of Equation 6.9(a) is higher than that of Equation 6.9(b).

$f_t = 0.137 \times f_c^{0.873}$ $R^2 = 0.9331$ 6.9(a)

$f_t = 0.557 \times \sqrt{f_c}$ $R^2 = 0.8249$ 6.9(b)

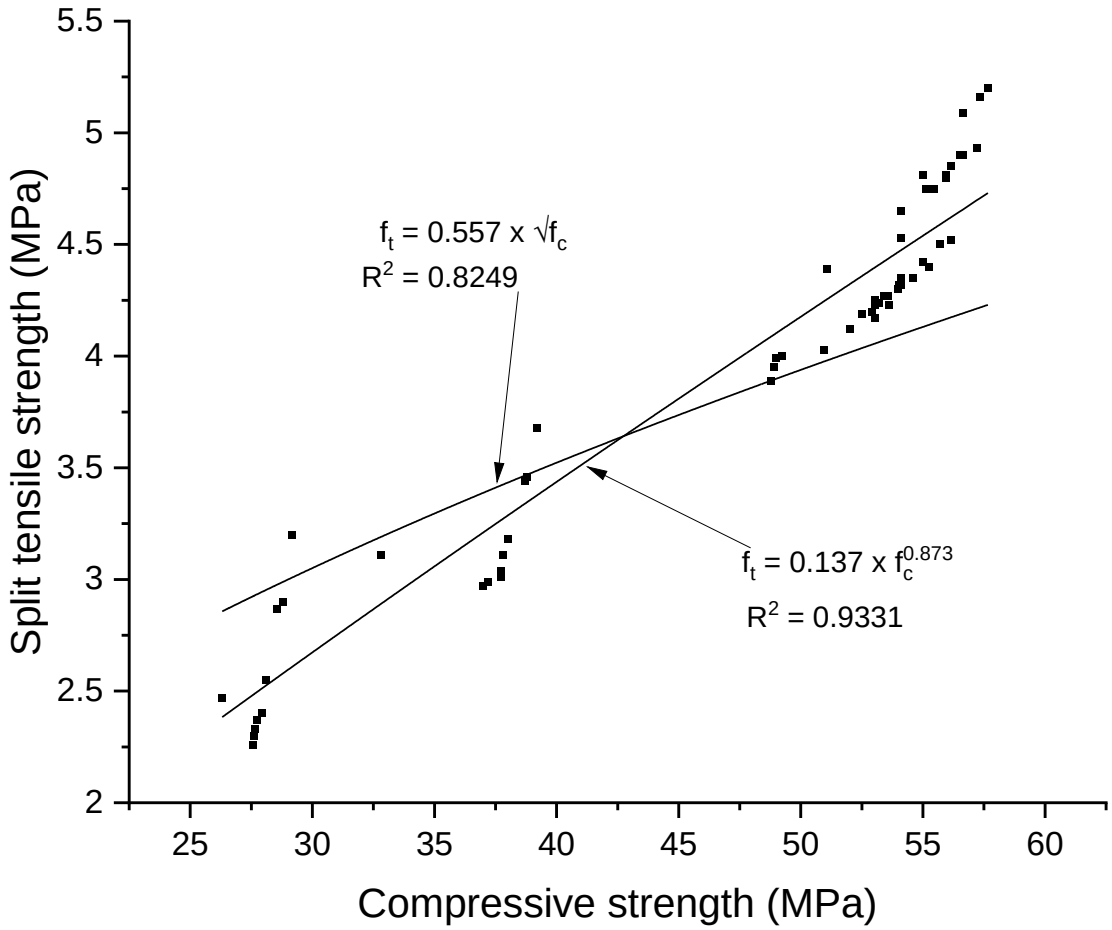

Figure 6.21 Comparison between compressive strength (f_c) and split tensile strength (f_t)

In order to make a comparison between various studies dealing with conversion of characteristic compressive strength (f_c) to characteristic split tensile strength (f_t), relationship as shown in Table 6.14 becomes useful [306]–[310].

Table 6.14 Empirical relationships between characteristic compressive and split tensile strength

Source	Empirical Expression	Equation No.
Zain et al. [306]	$f_t = \frac{f_{cc}}{0.1 \times f_{cc} + 7.11}$	6.10
Neville [307]	$f_t = 0.23 \times f_{cc}^{0.67}$	6.11
ACI 363R-92 [308]	$f_t = 0.59 \times \sqrt{f_{cc}}$	6.12
ACI 318-99 [309]	$f_t = 0.56 \times \sqrt{f_{cc}}$	6.13
CEB-199 [310]	$f_t = 0.30 \times f_{cc}^{0.67}$	6.14

Table 6.15 compares the 28 days split tensile strength of RSA and MS admixed concrete obtained through experiment with that derived through Equations 6.9(a) and (b) and equations given in Table 6.14. On comparing split tensile strength obtained from Equation 6.9(a) and (b), it can be observed that Equation 6.9(a) gave better results as compared to Equation 6.9(b) which was evident from the higher coefficient of determination. Therefore, it can be said with certainty that for predicting split tensile strength of RSA and MS admixed concrete from respective compressive strength, Equation 6.9(a) will be more accurate for all curing ages. Also, all the other equations provided predicted split tensile strength values accurately to experimental split tensile strength (with ratio close to 1) however, the results from Equation 6.9(b) and Equation 6.11 were on the lower side from the experimental observations.

Table 6.15 Comparison of different characteristic compressive-split tensile strength equations

Mix	Experimental Strength (MPa)			Predicted Split Tensile Strength (MPa) from Equations							Ratio of Experimental & Predicted Split Tensile Strength						
	f_c	f_{cc}= 0.8× f_c	f_t	6.9(a)	6.9(b)	6.10	6.11	6.12	6.13	6.14	$\frac{f_t}{6.9(a)}$	$\frac{f_t}{6.9(b)}$	$\frac{f_t}{6.10}$	$\frac{f_t}{6.11}$	$\frac{f_t}{6.12}$	$\frac{f_t}{6.13}$	$\frac{f_t}{6.14}$
R0	48.77	39.01	3.89	4.08	2.92	4.07	3.11	4.12	3.91	4.06	0.95	1.33	0.96	1.25	0.94	0.99	0.96
R10	48.88	39.10	3.95	4.08	2.93	4.07	3.11	4.12	3.92	4.06	0.97	1.35	0.97	1.27	0.96	1.01	0.97
M2.5	53.02	42.42	4.17	4.38	2.95	4.27	3.29	4.3	4.08	4.29	0.95	1.41	0.98	1.27	0.97	1.02	0.97
M5	54.08	43.26	4.53	4.46	2.99	4.32	3.33	4.34	4.12	4.35	1.02	1.52	1.05	1.36	1.04	1.1	1.04
M7.5	55.01	44.00	4.81	4.53	3.01	4.36	3.37	4.38	4.15	4.4	1.06	1.60	1.1	1.43	1.1	1.16	1.09
M10	51.07	40.86	4.39	4.24	2.86	4.18	3.21	4.22	4	4.18	1.04	1.54	1.05	1.37	1.04	1.1	1.05
R5M5	50.96	40.77	4.03	4.24	2.94	4.17	3.2	4.21	4	4.18	0.95	1.37	0.97	1.26	0.96	1.01	0.96
R5M7.5	53.61	42.89	4.23	4.43	2.98	4.3	3.31	4.32	4.1	4.32	0.95	1.42	0.98	1.28	0.98	1.03	0.98
R10M5	48.99	39.20	3.99	4.09	2.93	4.08	3.12	4.13	3.92	4.07	0.98	1.36	0.98	1.28	0.97	1.02	0.98
R10M7.5	49.22	39.38	4	4.11	2.93	4.09	3.13	4.14	3.93	4.08	0.97	1.36	0.98	1.28	0.97	1.02	0.98

6.9.4 Relationship between Flexural and Split Tensile Strength

The mathematical relationship between flexural and split tensile strength of M40 grade pavement quality concrete haven't been given much emphasis by the researchers in the past. Thus a relation between the two was suggested as shown in Equation 6.15(a) and (b). Figure 6.22 shows the variation of flexural strength ('f_r') with the split tensile strength ('f_t) for all days of curing.

$$f_r = 2.295 \times f_t^{0.6923} \qquad R^2 = 0.9445 \qquad 6.15(a)$$

$$f_r = 3 \times \sqrt{f_t} \qquad R^2 = 0.8796 \qquad 6.15(b)$$

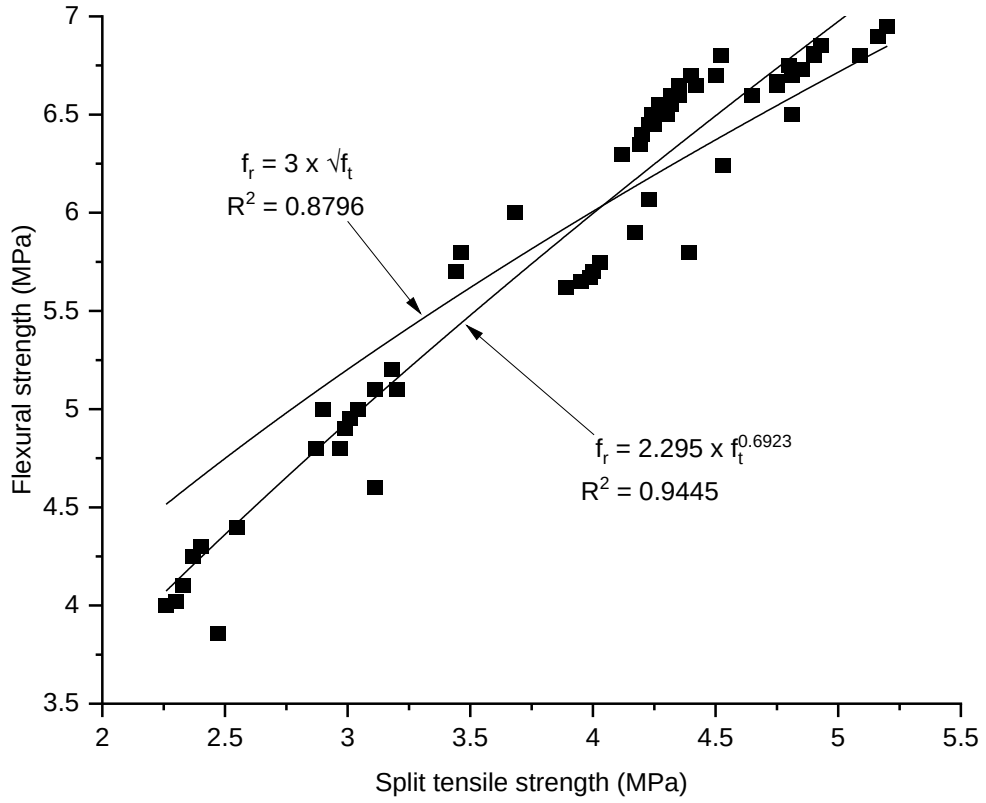

Figure 6.22 Comparison between flexural strength (f_r) and split tensile strength (f_t)

It can be observed that Equation 6.15(a) had higher coefficient of determination as compared to that of Equation 6.15(b). Therefore, it can be said with certainty that for predicting flexural strength of RSA and MS admixed concrete from respective split

tensile strength, Equation 6.15(a) will be more accurate for all curing ages. Also, the coefficient of determination of equations between flexural-compressive strength (Equation 6.2(a)) and split tensile-compressive strength (Equation 6.9(a)) were lower than the equation between flexural-split tensile strength (Equation 6.15(a)). It means that the mathematical relation between flexural-split tensile strength will give a more precise result as compared to the mathematical relation between flexural-compressive strength and split tensile-compressive strength.

6.10 CONCLUSIONS

The experiments performed in this chapter to analyse the mechanical strength of cement concrete admixed with RSA and MS led to the following conclusions:

- R10 (10% rice straw ash) showed only marginal strength gain w.r.t the control mix.

- Admixing of microsilica improved the compressive, flexural and split tensile strength of the concrete w.r.t. the control mix at all curing age except for compressive and flexural strength of the mix M10 (10% microsilica) at 3 and 7 days of curing. M7.5 (7.5% microsilica) gives the maximum strength amongst all the concrete mixes tested in this study.

- There was also an improvement in the strength of concrete when OPC was replaced with rice straw ash-microsilica composite. Amongst the concrete mixes admixed with rice straw ash-microsilica composite, R5M7.5 (5% rice straw ash-7.5% microsilica) had the maximum compressive, flexural and tensile strength.

- The strength gain in concrete due to admixing of microsilica was more as compared to admixing of rice straw ash.

- The mathematical relationships between various strengths of every concrete mix and their curing age were defined by logarithmic equations with a high coefficient of determination (R^2).

- The relationships between compressive-flexural strength ($f_r = 0.87 \times \sqrt{f_c}$ for 28 days of curing and $f_r = 0.561 \times f_c^{0.615}$ for other days of curing) and compressive-split tensile strength ($f_t = 0.137 \times$ $^{0.873}$ for all days of curing) were defined by power equations with high coefficient of determination (R^2). These equations were compared with the equations given by other researchers and various specifications of different countries and were found to be more accurate in case of concrete admixed with rice straw ash and microsilica.

- Mineralogical analysis (XRD) and microstructural analysis (SEM and petrography) established the results obtained from the compressive, flexural and split tensile strength tests of different concrete mixes.